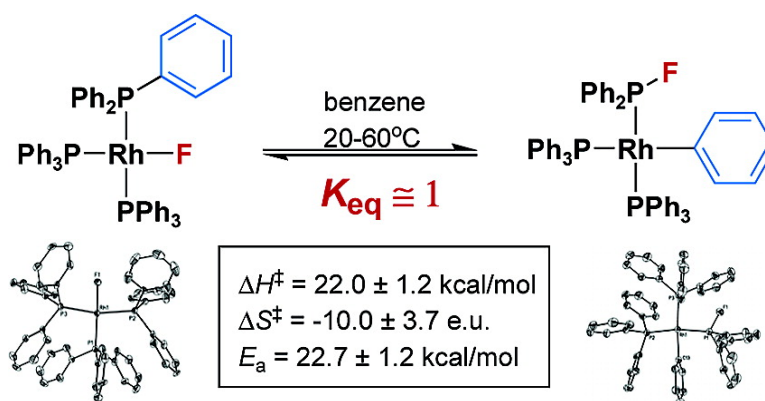


The F/Ph Rearrangement Reaction of [(PhP)RhF], the Fluoride Congener of Wilkinson's Catalyst

Stuart A. Macgregor, D. Christopher Roe, William J. Marshall,
 Karen M. Bloch, Vladimir I. Bakhmutov, and Vladimir V. Grushin

J. Am. Chem. Soc., **2005**, 127 (43), 15304-15321 • DOI: 10.1021/ja054506z • Publication Date (Web): 08 October 2005

Downloaded from <http://pubs.acs.org> on March 25, 2009



More About This Article

Additional resources and features associated with this article are available within the HTML version:

- Supporting Information
- Links to the 15 articles that cite this article, as of the time of this article download
- Access to high resolution figures
- Links to articles and content related to this article
- Copyright permission to reproduce figures and/or text from this article

[View the Full Text HTML](#)

The F/Ph Rearrangement Reaction of $[(\text{Ph}_3\text{P})_3\text{RhF}]$, the Fluoride Congener of Wilkinson's Catalyst

Stuart A. Macgregor,^{*,‡} D. Christopher Roe,[†] William J. Marshall,[†] Karen M. Bloch,[†] Vladimir I. Bakhmutov,[§] and Vladimir V. Grushin^{*,†}

Contribution from Central Research & Development, E. I. DuPont de Nemours and Company, Inc., Experimental Station, Wilmington, Delaware 19880-0328, School of Engineering and Physical Sciences, William H. Perkin Building, Heriot-Watt University, Edinburgh EH14 4AS, U.K., and Department of Chemistry, Texas A&M University, P.O. Box 30012, College Station, Texas 77842-3012

Received July 7, 2005; E-mail: vlad.grushin-1@usa.dupont.com; s.a.macgregor@hw.ac.uk

Abstract: The fluoride congener of Wilkinson's catalyst, $[(\text{Ph}_3\text{P})_3\text{RhF}]$ (**1**), has been synthesized and fully characterized. Unlike Wilkinson's catalyst, **1** easily activates the inert C–Cl bond of ArCl (Ar = Ph, *p*-tolyl) under mild conditions (3 h at 80 °C) to produce *trans*- $[(\text{Ph}_3\text{P})_2\text{Rh}(\text{Ph}_2\text{PF})(\text{Cl})]$ (**2**) and ArPh as a result of C–Cl, Rh–F, and P–C bond cleavage and C–C, Rh–Cl, and P–F bond formation. In benzene (2–3 h at 80 °C), **1** decomposes to a 1:1 mixture of *trans*- $[(\text{Ph}_3\text{P})_2\text{Rh}(\text{Ph}_2\text{PF})(\text{F})]$ (**3**) and the cyclometalated complex $[(\text{Ph}_3\text{P})_2\text{Rh}(\text{Ph}_2\text{PC}_6\text{H}_4)]$ (**4**). Both the chloroarene activation and the thermal decomposition reactions have been shown to occur via the facile and reversible F/Ph rearrangement reaction of **1** to *cis*- $[(\text{Ph}_3\text{P})_2\text{Rh}(\text{Ph})(\text{Ph}_2\text{PF})]$ (**5**), which has been isolated and fully characterized. Kinetic studies of the F/Ph rearrangement, an intramolecular process not influenced by extra phosphine, have led to the determination of $E_a = 22.7 \pm 1.2 \text{ kcal mol}^{-1}$, $\Delta H^\ddagger = 22.0 \pm 1.2 \text{ kcal mol}^{-1}$, and $\Delta S^\ddagger = -10.0 \pm 3.7 \text{ eu}$. Theoretical studies of F/Ph exchange with the $[(\text{PH}_3)_2(\text{PH}_2\text{Ph})\text{RhF}]$ model system pointed to two possible mechanisms: (i) Ph transfer to Rh followed by F transfer to P (formally oxidative addition followed by reductive elimination, pathway 1) and (ii) F transfer to produce a metallophosphorane with subsequent Ph transfer to Rh (pathway 2). Although pathway 1 cannot be ruled out completely, the metallophosphorane mechanism finds more support from both our own and previously reported observations. Possible involvement of metallophosphorane intermediates in various P–F, P–O, and P–C bond-forming reactions at a metal center is discussed.

Introduction

The chemistry of late transition metal fluoride complexes has constituted a new and expanding area for research in recent years.^{1–7} In addition to interesting applications in synthesis and catalysis,^{8–16} C–H activation,¹⁷ materials science,¹⁸ and the

generation of highly reactive “naked” fluoride,¹⁹ late transition metal fluorides have attracted much attention due to their uncommon chemical properties and bonding features.^{1,5,7,20–52}

[†] DuPont CR&D.

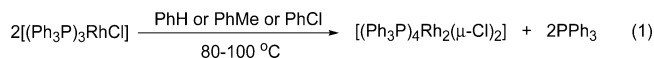
[‡] Heriot-Watt University.

[§] Texas A&M University.

- (1) Doherty, N. M.; Hoffmann, N. W. *Chem. Rev.* **1991**, *91*, 553.
- (2) Holloway, J. H.; Hope, E. G. *J. Fluorine Chem.* **1996**, *76*, 209.
- (3) Murphy, E. F.; Murugavel, R.; Roesky, H. W. *Chem. Rev.* **1997**, *97*, 3425.
- (4) Clark, H. C. S.; Holloway, J. H. *Adv. Inorg. Fluorides* **2000**, 51.
- (5) Mezzetti, A.; Becker, C. *Helv. Chim. Acta* **2002**, *85*, 2686. Also, see: Becker, C.; Kieltisch, I.; Brogini, D.; Mezzetti, A. *Inorg. Chem.* **2003**, *42*, 8417.
- (6) Braun, T.; Perutz, R. N. *Chem. Commun.* **2002**, 2749.
- (7) Grushin, V. V. *Chem. Eur. J.* **2002**, *8*, 1006.
- (8) Vaska, L.; Peone, J., Jr. *J. Chem. Soc., Chem. Commun.* **1971**, 418. Vaska, L.; Peone, J., Jr. *Inorg. Synth.* **1974**, *15*, 64.
- (9) Jones, C. M.; Doherty, N. M. *Polyhedron* **1995**, *14*, 81.
- (10) Cooper, A. C.; Caulton, K. G. *Inorg. Chim. Acta* **1996**, *251*, 41.
- (11) Cooper, A. C.; Huffman, J. C.; Caulton, K. G. *Inorg. Chim. Acta* **1998**, *270*, 261.
- (12) Dorta, R.; Egli, P.; Zuercher, F.; Togni, A. *J. Am. Chem. Soc.* **1997**, *119*, 10857.
- (13) Krueger, J.; Carreira, E. M. *J. Am. Chem. Soc.* **1998**, *120*, 837.
- (14) Barshay, P.; Togni, A.; Mezzetti, A. *Organometallics* **2001**, *20*, 3472.
- (15) Vicente, J.; Gil-Rubio, J.; Guerrero-Leal, J.; Bautista, D. *Organometallics* **2004**, *23*, 4871.
- (16) Renkema, K. B.; Werner-Zwanziger, U.; Pagel, M. D.; Caulton, K. G. *J. Mol. Catal. A* **2004**, *224*, 125.
- (17) Cooper, A. C.; Foltig, K.; Huffman, J. C.; Caulton, K. G. *Organometallics* **1997**, *16*, 505.
- (18) Lobban, J. International Patent Application WO 2003089443 A1, 2003.
- (19) Grushin, V. V. *Angew. Chem., Int. Ed.* **1998**, *37*, 994.
- (20) Poulton, J. T.; Sigalas, M. P.; Eisenstein, O.; Caulton, K. G. *Inorg. Chem.* **1993**, *32*, 5490.
- (21) Poulton, J. T.; Sigalas, M. P.; Foltig, K.; Streib, W. E.; Eisenstein, O.; Caulton, K. G. *Inorg. Chem.* **1994**, *33*, 1476.
- (22) Cooper, A. C.; Bollinger, J. C.; Huffman, J. C.; Caulton, K. G. *New J. Chem.* **1998**, *22*, 473.
- (23) Coalter, J. N., III; Huffman, J. C.; Streib, W. E.; Caulton, K. G. *Inorg. Chem.* **2000**, *39*, 3757.
- (24) Huang, D.; Koren, P. R.; Foltig, K.; Davidson, E. R.; Caulton, K. G. *J. Am. Chem. Soc.* **2000**, *122*, 8916.
- (25) Caulton, K. G. *New J. Chem.* **1994**, *18*, 25.
- (26) Veltheer, J. E.; Burger, P.; Bergman, R. G. *J. Am. Chem. Soc.* **1995**, *117*, 12478.
- (27) Fraser, S. L.; Antipin, M. Yu.; Khroustalyov, V. N.; Grushin, V. V. *J. Am. Chem. Soc.* **1997**, *119*, 4769.
- (28) Pilon, M. C.; Grushin, V. V. *Organometallics* **1998**, *17*, 1774.
- (29) Flemming, J. P.; Pilon, M. C.; Borbulevitch, O. Ya.; Antipin, M. Yu.; Grushin, V. V. *Inorg. Chim. Acta* **1998**, *280*, 87.
- (30) Marshall, W. J.; Thorn, D. L.; Grushin, V. V. *Organometallics* **1998**, *17*, 5427.
- (31) Grushin, V. V. *Organometallics* **2000**, *19*, 1888.
- (32) Grushin, V. V.; Marshall, W. J. *Angew. Chem., Int. Ed.* **2002**, *41*, 4476.
- (33) Marshall, W. J.; Grushin, V. V. *Organometallics* **2003**, *22*, 555.
- (34) Marshall, W. J.; Grushin, V. V. *Organometallics* **2004**, *23*, 3343.
- (35) Clark, H. C. S.; Fawcett, J.; Holloway, J. H.; Hope, E. G.; Peck, L. A.; Russell, D. R. *J. Chem. Soc., Dalton Trans.* **1998**, 1249.

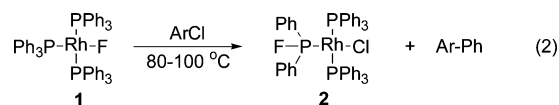
It is now recognized that fluoro transition metal complexes are distinctive, exhibiting reactivity patterns that are remarkably different from those of their much better known chloro, bromo, and iodo counterparts. This statement is strongly supported, for example, by the fluoro congener of Wilkinson's catalyst, $[(\text{Ph}_3\text{P})_3\text{RhF}]$ (**1**).

Recently, an efficient, simple synthesis of **1** was communicated along with its full characterization and unexpected reactivity.⁵³ On one hand, **1** appeared akin to its famous counterpart $[(\text{Ph}_3\text{P})_3\text{RhCl}]$ (Wilkinson's catalyst),⁵⁴ in that both displayed (i) similar geometry parameters in the solid state, (ii) the same degree of phosphine dissociation in solution, and (iii) the ability to decarbonylate DMF to give $[(\text{Ph}_3\text{P})_2\text{Rh}(\text{CO})\text{X}]$ ($\text{X} = \text{F}$ or Cl).⁵³ On the other hand, both the thermal decomposition of **1** in benzene and the reaction of **1** with chlorobenzene or 4-chlorotoluene take paths that are not even remotely similar to the reactivity of Wilkinson's catalyst under identical conditions. It is known⁵⁴ that heating $[(\text{Ph}_3\text{P})_3\text{RhCl}]$ in benzene or toluene leads to precipitation of $[(\text{Ph}_3\text{P})_4\text{Rh}_2(\mu\text{-Cl})_2]$ due to PPh_3 dissociation. The same dinuclear complex was also produced in >95% selectivity when the reaction was performed in chlorobenzene (100 °C, 2.5 h, eq 1) with only trace amounts (<2%) of the oxidative addition product $[(\text{Ph}_3\text{P})_2\text{-Rh}(\text{Ph})\text{Cl}_2]$ being detected by ³¹P NMR.⁵³ This is not surprising because activation of the notoriously inert C–Cl bond of PhCl and other unactivated chloroarenes with a Rh(I) or Pd(0) species normally occurs only when the metal center bears a tertiary phosphine that is bulkier and more electron rich than PPh_3 .⁵⁵



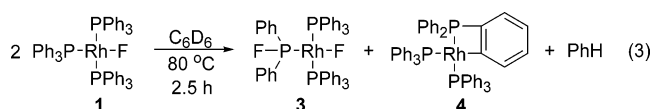
In sharp contrast,^{55a} **1** was found to easily cleave the C–Cl bond of chlorobenzene and *p*-chlorotoluene (TolCl) under unexpectedly mild conditions (1–3 h at 80–100 °C), as shown in eq 2.⁵³ This reaction gave rise to a new Rh(I) complex, *trans*-

$[(\text{Ph}_3\text{P})_2\text{Rh}(\text{Ph}_2\text{PF})(\text{Cl})]$ (**2**), as a result of C–Cl, Rh–F, and P–C bond cleavage and C–C, Rh–Cl, and P–F bond formation. This unusual result provides an interesting comparison with the “normal” oxidative addition of iodobenzene^{53,56} and *p*-iodotoluene⁵⁷ to the chloro and iodo analogues of **1**. First, despite the much higher reactivity of the C–I bond, the reactions of $[(\text{Ph}_3\text{P})_3\text{RhX}]$ ($\text{X} = \text{Cl}, \text{I}$) with PhI or TolI require higher temperatures and longer reaction times to occur. Second, the latter reactions lead to the formation of the expected oxidative addition products, σ -aryl Rh(III) complexes $[(\text{Ph}_3\text{P})_2\text{-Rh}(\text{Ar})\text{X}_2]$, as a result of Ar–I bond cleavage and Rh–I and Rh–Ar bond formation.^{53,56,57}



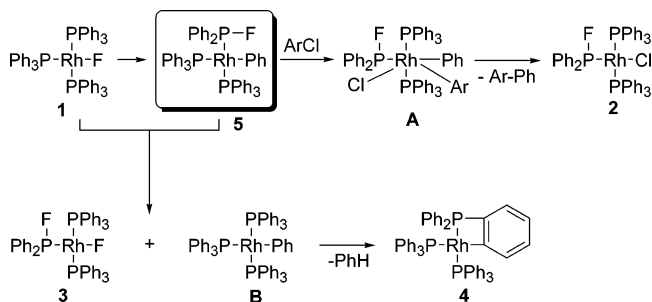
Ar = Ph or Tol

Equally unexpected were both the ease and the outcome of the thermal decomposition of **1** in benzene (eq 3).⁵³ After 2–3 h at 80 °C, **1** was smoothly converted to a 1:1 mixture of *trans*- $[(\text{Ph}_3\text{P})_2\text{Rh}(\text{Ph}_2\text{PF})(\text{F})]$ (**3**) containing Rh–F and P–F bonds, and the long-known⁵⁸ cyclometalated complex **4**.



To account for the results described in eqs 2 and 3, a unifying mechanistic scheme was proposed, involving rearrangement of **1** to $[(\text{Ph}_3\text{P})_2\text{Rh}(\text{Ph})(\text{Ph}_2\text{PF})]$ (**5**; *cis* or *trans*) as the first key step (Scheme 1).⁵³ If the fluorine and a phenyl in **1** interchanged their positions, a σ -phenyl Rh(I) species would be formed (such as **5**), which one might expect⁵⁹ to be electron-rich enough to

Scheme 1



- (36) Tilset, M.; Fjeldahl, I.; Hamon, J.-R.; Hamon, P.; Toupet, L.; Saillard, J.-Y.; Costuas, K.; Haynes, A. *J. Am. Chem. Soc.* **2001**, *123*, 9984. Tilset, M.; Hamon, J.-R.; Hamon, P. *Chem. Commun.* **1998**, 765.
- (37) (a) Cronin, L.; Higgitt, C. L.; Karch, R.; Perutz, R. N. *Organometallics* **1997**, *16*, 4920. (b) Braun, T.; Parsons, S.; Perutz, R. N.; Voith, M. *Organometallics* **1999**, *18*, 1710.
- (38) Jasim, N. A.; Perutz, R. N.; Foxon, S. P.; Walton, P. H. *J. Chem. Soc., Dalton Trans.* **2001**, 1676.
- (39) Jasim, N. A.; Perutz, R. N.; Archibald, S. J. *Dalton Trans.* **2003**, 2184.
- (40) Reinhold, M.; McGrady, J. E.; Perutz, R. N. *J. Am. Chem. Soc.* **2004**, *126*, 5268.
- (41) Gil-Rubio, J.; Weberndorfer, B.; Werner, H. *J. Chem. Soc., Dalton Trans.* **1999**, 1437.
- (42) Moigno, D.; Callejas-Gaspar, B.; Gil-Rubio, J.; Werner, H.; Kiefer, W. *J. Organomet. Chem.* **2002**, *661*, 181.
- (43) Gorol, M.; Moesch-Zanetti, N. C.; Roesky, H. W.; Noltemeyer, M.; Schmidt, H.-G. *Eur. J. Inorg. Chem.* **2004**, 2678.
- (44) Barthazy, P.; Hintermann, L.; Stoop, R. M.; Worle, M.; Mezzetti, A.; Togni, A. *Helv. Chim. Acta* **1999**, *82*, 2448. Barthazy, P.; Stoop, R. M.; Woerle, M.; Togni, A.; Mezzetti, A. *Organometallics* **2000**, *19*, 2844.
- (45) Barthazy, P.; Brogini, D.; Mezzetti, A. *Can. J. Chem.* **2001**, *79*, 904.
- (46) Kirkham, M. S.; Mahon, M. F.; Whittlesey, M. K. *Chem. Commun.* **2001**, 813.
- (47) Braun, T.; Noveski, D.; Neumann, B.; Stammler, H.-G. *Angew. Chem., Int. Ed.* **2002**, *41*, 2745.
- (48) Noveski, D.; Braun, T.; Schulte, M.; Neumann, B.; Stammler, H.-G. *Dalton Trans.* **2003**, 4075.
- (49) Noveski, D.; Braun, T.; Kruckemeier, S. J. *Fluorine Chem.* **2004**, *125*, 959.
- (50) Nilsson, P.; Plamper, F.; Wendt, O. F. *Organometallics* **2003**, *22*, 5235.
- (51) (a) Yahav, A.; Goldberg, I.; Vigalok, A. *J. Am. Chem. Soc.* **2003**, *125*, 13634. (b) Yahav, A.; Goldberg, I.; Vigalok, A. *Inorg. Chem.* **2005**, *44*, 1547.
- (52) Vicente, J.; Gil-Rubio, J.; Bautista, D.; Sironi, A.; Masciocchi, N. *Inorg. Chem.* **2004**, *43*, 5665.
- (53) Grushin, V. V.; Marshall, W. J. *J. Am. Chem. Soc.* **2004**, *126*, 3068.
- (54) Jardine, F. H. *Prog. Inorg. Chem.* **1981**, *28*, 63.

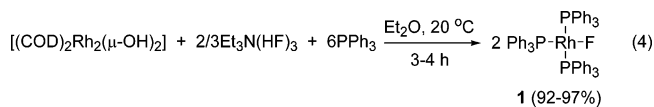
- (55) (a) For reviews, see: Grushin, V. V.; Alper, H. *Chem. Rev.* **1994**, *94*, 1047; *Top. Organomet. Chem.* **1999**, *3*, 193. (b) For the earliest original contributions to Pd/dipp-catalyzed reactions of nonactivated chloroarenes from Milstein's group, see: Ben-David, Y.; Portnoy, M.; Milstein, D. *J. Am. Chem. Soc.* **1989**, *111*, 8742; *J. Chem. Soc., Chem. Commun.* **1989**, 1816. For a full citation of Milstein's catalytic Ar–Cl activation work, see ref 55a. (c) For the original contribution to CysP/Pd -catalyzed reactions of chlorobenzene from Osborn's group, see: Huser, M.; Youinou, M. T.; Osborn, J. A. *Angew. Chem., Int. Ed. Engl.* **1989**, *28*, 1386. For a full citation of Osborn's catalytic Ar–Cl activation work, see ref 55a. (d) For early work on Ar–Cl activation, catalyzed by Rh complexes of bulky, basic phosphines, see: Grushin, V. V.; Alper, H. *Organometallics* **1991**, *10*, 1620. (e) For the discovery of the currently most popular *t*-Bu₃P–Pd catalytic system for chloroarene activation, see: Nishiyama, M.; Koie, Y. *Eur. Pat. Appl. EP 802173 A1*, 1997. Yamamoto, T.; Nishiyama, M.; Koie, Y. *Tetrahedron Lett.* **1998**, *39*, 617 and 2367. More recently, *t*-Bu₃P has been widely and successfully used by Littke and Fu for various Pd-catalyzed cross-coupling reactions of chloroarenes.^{55f} For a review, see: Littke, A. F.; Fu, G. C. *Angew. Chem., Int. Ed.* **2002**, *41*, 4176.

oxidatively add the C–Cl bond of chlorobenzene. A separate experiment did indicate⁵³ that $[(\text{Ph}_3\text{P})_3\text{RhPh}]$ ⁵⁸ readily reacted with PhCl (neat; 80 °C; <1 h) to give $[(\text{Ph}_3\text{P})_3\text{RhCl}]$ and Ph₂ apparently via C–Cl oxidative addition and C–C reductive elimination. Therefore, it seemed reasonable to propose that **5** would react with ArCl to produce **A**, followed by C–C reductive elimination from **A** to give Ar–Ph and **2** (Scheme 1), both of which were indeed the products of the reaction (eq 2). In the absence of ArCl or any other reactive electrophile, **5** might undergo P–ligand exchange with the as yet unreacted **1** (Scheme 1), resulting in the observed difluoride **3** (eq 3) and $[(\text{Ph}_3\text{P})_3\text{RhPh}]$ ⁵⁸ (**B**). The latter was previously found⁵³ to undergo rapid and clean cyclometalation to **4** even below 80 °C.

Although the proposed F/Ph rearrangement did account for the reactivity of **1**, no evidence was obtained for the intermediate formation of **5**, as shown in Scheme 1.⁵³ To establish the mechanism of these uncommon reactions of **1** (eqs 2 and 3), we undertook a detailed investigation of this chemistry. As a result of these studies, the previously proposed F/Ph exchange reaction of **1** was indeed observed. In this paper, we report the remarkably facile and reversible rearrangement of $[(\text{Ph}_3\text{P})_3\text{RhF}]$, **1**, to $[(\text{Ph}_3\text{P})_2\text{Rh}(\text{Ph})(\text{Ph}_2\text{PF})]$, **5** (cis form), and the results of both experimental and theoretical studies of this intriguing exchange.

Results

Synthesis and Reactivity of $[(\text{Ph}_3\text{P})_3\text{RhF}]$ (1**).** The fluoro analogue of Wilkinson's catalyst $[(\text{Ph}_3\text{P})_3\text{RhF}]$, **1**, has been previously mentioned in the literature,^{9,60} although without proper characterization. We found that **1** can be effortlessly prepared by reacting easily accessible $[(\text{COD})_2\text{Rh}_2(\mu\text{-OH})_2]$ ⁶¹ with $\text{Et}_3\text{N}(\text{HF})_3$ (TREAT HF)⁶² and excess PPh₃ in ether (eq 4). This method furnished analytically pure **1** as an orange-yellow powder, which precipitated from the reaction mixture in almost quantitative yield. Multigram quantities of **1** were prepared using reaction 4. Less conveniently, **1** was synthesized by reacting $[(\text{PPh}_3)_4\text{Rh}_2(\mu\text{-OH})_2]$ ⁶³ with TREAT HF to give $[(\text{PPh}_3)_4\text{Rh}_2(\mu\text{-F})_2]$,⁵³ which transformed to **1** upon treatment with PPh₃.



Complex **1** is air-sensitive, especially in solution. It is moderately soluble in benzene (ca. 0.6 g in 100 mL at 25 °C), poorly soluble in toluene and THF, and insoluble in ether, alkanes, and cycloalkanes. Chlorinated solvents such as dichloromethane and chloroform were found to cause rapid decomposition of **1**. Like Wilkinson's catalyst,⁵⁴ **1** also loses PPh₃ in benzene solution, producing $[(\text{PPh}_3)_4\text{Rh}_2(\mu\text{-F})_2]$ (eq 5). This process is reversible, with the equilibrium being established within the time of dissolution. The degree of phosphine

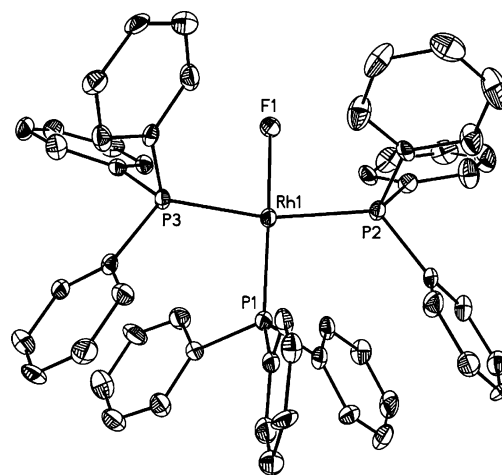
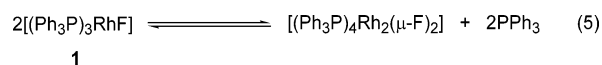


Figure 1. ORTEP drawing of **1** with thermal ellipsoids drawn to the 50% probability level and all H atoms omitted for clarity.

Table 1. Geometry Parameters for **1** and $[(\text{Ph}_3\text{P})_3\text{RhCl}]$

parameter, Å or deg	$[(\text{Ph}_3\text{P})_3\text{RhF}]$, 1 (this work)	$[(\text{Ph}_3\text{P})_3\text{RhCl}]$ (ref 64)	
		orange	red
Rh–X	2.070(2)	2.404(4)	2.376(4)
Rh–P trans to X	2.193(1)	2.225(4)	2.214(4)
Rh–P trans to P	2.325(1)	2.304(4)	2.322(4)
Rh–P trans to P	2.325(1)	2.338(4)	2.334(4)
X–Rh–P	166.9(1)	166.7(2)	156.2(2)
P–Rh–P	159.7(1)	159.1(2)	152.8(1)

dissociation from **1** (eq 5) in rigorously anhydrous benzene (25 °C) was determined by ³¹P NMR and calculated at ca. 30%, similar to the value measured for Wilkinson's catalyst under identical conditions. In the solid state, **1** revealed a square-planar geometry around Rh (Figure 1), with the coordination bond angles and distances being strikingly similar to those⁶⁴ of both the red and the orange forms of Wilkinson's catalyst (Table 1).



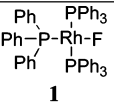
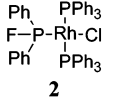
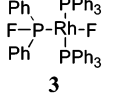
Heating **1** in chlorobenzene at 80 °C for 2–3 h resulted in the formation of *trans*- $[(\text{Ph}_3\text{P})_2\text{Rh}(\text{Ph}_2\text{PF})(\text{Cl})]$ (**2**) and biphenyl, as shown in eq 2. Repeating the experiment in 4-chlorotoluene produced 4-methylbiphenyl instead of Ph₂ (eq 2). Complex **2** was isolated and fully characterized by X-ray analysis (Figure 2) and NMR data (Table 2). The formation of biphenyl and 4-methylbiphenyl was confirmed by GC–MS.⁵³

Fluoride **1** also readily reacted with iodobenzene and bromobenzene. In both cases, the reaction produced Rh(III) complexes $[(\text{Ph}_3\text{P})_2\text{Rh}(\text{Ph})\text{X}_2]$, where X = I or Br, respectively.⁵³ It is likely that these reactions first produced $[(\text{Ph}_3\text{P})_2\text{Rh}(\text{Ph}_2\text{PF})(\text{X})]$ (X = I or Br), much like the reaction of **1** with PhCl (eq 2). Being much more reactive than PhCl, however, PhI and PhBr would oxidatively add to the initially generated $[(\text{Ph}_3\text{P})_2\text{Rh}(\text{Ph}_2\text{PF})(\text{X})]$ to give $[(\text{Ph}_3\text{P})_2\text{Rh}(\text{Ph})\text{X}_2]$, a stable and isolable Rh(III) species (eq 6). Both $[(\text{Ph}_3\text{P})_2\text{Rh}(\text{Ph})\text{Br}_2]$ and $[(\text{Ph}_3\text{P})_2\text{Rh}(\text{Ph})\text{I}_2]$ were structurally characterized by X-ray diffraction.⁵³ The fluorinated phosphine, Ph₂PF, that is lost in the second oxidative addition (eq 6) could not be observed due to its poor stability.⁶⁵ However, doublets with $J_{\text{P-F}} = 665, 838, 971, \text{ and } 1017 \text{ Hz}$ observed in the range of –35 to –81 ppm in

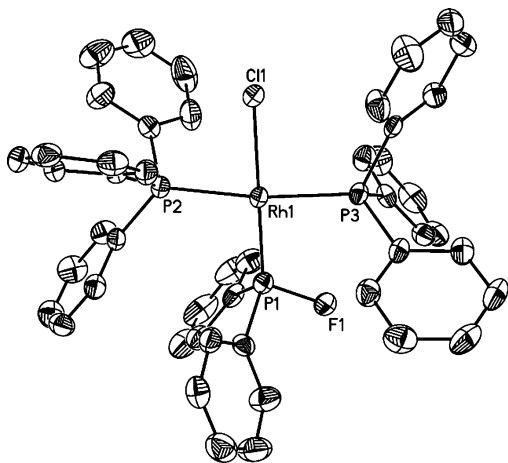
(64) Bennett, M. J.; Donaldson, P. B. *Inorg. Chem.* **1977**, *16*, 655.

(56) Mori, K.; Mizoroki, T.; Ozaki, T. *Bull. Chem. Soc. Jpn.* **1976**, *49*, 758.
 (57) Ishiyama, T.; Hartwig, J. J. *Am. Chem. Soc.* **2000**, *122*, 12043.
 (58) Keim, W. *J. Organomet. Chem.* **1968**, *14*, 179.
 (59) Semmelhack, M. F.; Ryono, L. *Tetrahedron Lett.* **1973**, *14*, 2967.
 (60) Van Gaal, H. L. M.; Van den Bekerom, F. L. A.; Verlaan, J. P. J. *J. Organomet. Chem.* **1976**, *114*, C35.
 (61) Uson, R.; Oro, L. A.; Cabeza, J. A. *Inorg. Synth.* **1985**, *23*, 126.
 (62) McClinton, M. A. *Aldrichimica Acta* **1995**, *28*, 31. Haufe, G. *J. Prakt. Chem.* **1996**, *338*, 99.
 (63) Grushin, V. V.; Kuznetsov, V. F.; Bensimone, C.; Alper, H. *Organometallics* **1995**, *14*, 3927.

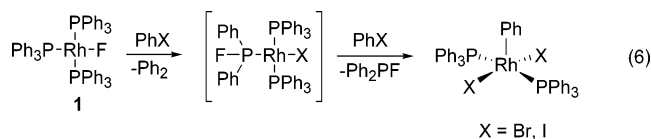
Table 2. ^{19}F and ^{31}P NMR Data for **1**, **2**, and **3** in Benzene- d_6 at 20 °C

	^{19}F NMR δ (ppm), J (Hz)	^{31}P NMR δ (ppm), J (Hz)
 1	-286.3 (ddt) ^a $J_{\text{F-Rh}} = 77.6$; $J_{\text{F-P(trans)}} = 172.4$; $J_{\text{F-P(cis)}} = 28.5$	32.4 (ddd, 2P) $J_{\text{P-Rh}} = 154.3$; $J_{\text{P-P}} = 39.0$; $J_{\text{P-F}} = 28.5$ 57.4 (ddt, 1P) $J_{\text{P-Rh}} = 181.4$; $J_{\text{P-P}} = 39.0$; $J_{\text{P-F}} = 172.4$
 2	-110.7 (ddt) $J_{\text{F-P}} = 856$; $J_{\text{P-P}} = 20.0$; $J_{\text{F-Rh}} = 14.1$	35.5 (ddd, 2P) $J_{\text{P-Rh}} = 139.0$; $J_{\text{P-P}} = 40.7$; $J_{\text{P-F}} = 20.0$ 181.4 (ddt, 1P) $J_{\text{P-F}} = 856$; $J_{\text{P-Rh}} = 222.1$; $J_{\text{P-P}} = 40.7$
 3	-109.7 (ddt, 1F) $J_{\text{F-P}} = 848$; $J_{\text{P-P}} = 30$; $J_{\text{F-Rh}} = 15$ -267.9 (ddt, 1F) $J_{\text{F-Rh}} = 58.5$; $J_{\text{F-P(trans)}} = 217$; $J_{\text{F-P(cis)}} = 27$	32.3 (dddd, 2P) $J_{\text{P-Rh}} = 150$; $J_{\text{P-P}} = 41.5$; $J_{\text{P-F}} = 27$; $J_{\text{P-F}} = 15$ 188.8 (dddt, 1P) $J_{\text{P-F}} = 848$; $J_{\text{P-P}} = 217$; $J_{\text{P-Rh}} = 207.4$; $J_{\text{P-P}} = 41.5$

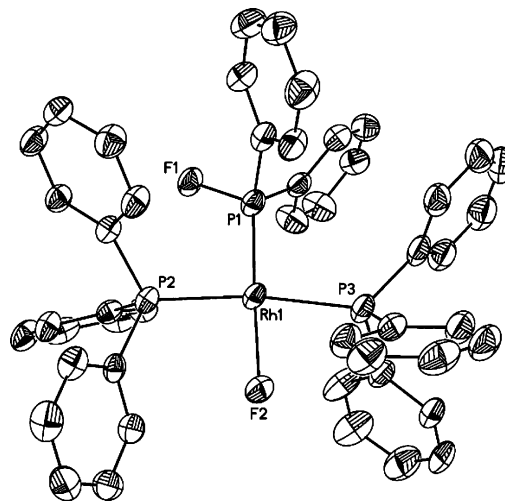
^a Coupling commonly observed in the presence of excess PPh_3 and/or anhydrous CsF .

**Figure 2.** ORTEP drawing of **2** with thermal ellipsoids drawn to the 50% probability level and all H atoms omitted for clarity.

the ^{19}F NMR spectra of the reaction mixtures provided firm evidence for P–F bond formation.



The thermal decomposition of **1** in benzene at 80 °C (eq 3) readily occurred to >90% conversion after 3 h. The ^{31}P and ^{19}F NMR spectra of the reaction mixture indicated that two complexes were cleanly produced, *trans*- $[(\text{Ph}_3\text{P})_2\text{Rh}(\text{Ph}_2\text{PF})(\text{F})]$ (**3**; see Table 2) and the cyclometalated complex **4**. The latter was identified by its characteristic ^{31}P NMR spectrum,⁶⁶ whereas the structure of the former (**3**) was established based on both the ^{31}P and the ^{19}F NMR data.⁵³ Fractional crystallization of the reaction mixture afforded X-ray quality crystals of **3** for structural characterization in the solid state (Figure 3). During these studies, it was also found that using cotton wool

**Figure 3.** ORTEP drawing of **3** with thermal ellipsoids drawn to the 50% probability level and all H atoms omitted for clarity.

for filtration of the reaction mixtures could lead to the formation of the bifluoride analogue of **3**, *trans*- $[(\text{Ph}_3\text{P})_2\text{Rh}(\text{Ph}_2\text{PF})(\text{FHF})]$, **6**, probably due to partial hydrolysis of **3** on the cotton surface. Although only small quantities of the bifluoride were produced, a few single crystals of **6** were obtained and found suitable for an X-ray diffraction study (Figure 4). Table 2 lists NMR data for the new complexes **1**, **2**, and **3**.

X-ray Structures of $[(\text{Ph}_3\text{P})_3\text{RhF}]$ and *trans*- $[(\text{Ph}_3\text{P})_2\text{Rh}(\text{Ph}_2\text{PF})(\text{X})]$ (X = Cl, F, and FHF). Table 3 provides coordination geometry parameters of the structurally related **1**, **2**, **3**, and **6**. A number of interesting conclusions can be drawn, as follows.

(1) The P–Rh bonds for the Ph_2PF ligands in **2**, **3**, and **6** are ca. 0.04–0.09 Å shorter than the Ph_3P –Rh bonds *trans* to X in **1** (X = F) and in Wilkinson's catalyst (X = Cl, see Table 1). The shorter bonds to the more π -acidic Ph_2PF ligand indicate an important contribution of metal to P π -back-donation⁶⁷ to the P–Rh bonding⁶⁸ involving an electron-rich metal center.

(2) The Rh–F bond is ca. 0.03 Å shorter when *trans* to Ph_2PF (**3**) rather than to PPh_3 (**1**). The importance of a π -acceptor *trans* to F for stabilization of the M–F bond in

(65) (a) Brown, C.; Murray, M.; Schmutzler, R. *J. Chem. Soc. C* **1970**, 878. (b) Riesel, L.; Haenel, J.; Ohms, G. *J. Fluorine Chem.* **1988**, *38*, 335.

(66) Kuznetsov, V. F.; Yap, G. P. A.; Bensimon, C.; Alper, H. *Inorg. Chim. Acta* **1998**, *280*, 172.

Table 3. Selected Geometry Parameters for 1, 2, 3, and 6

Complex	Ph ² PPh ₃ Ph-P ¹ -Rh-F Ph ³ PPh ₃ 1	Ph ² PPh ₃ F-P ¹ -Rh-Cl Ph ³ PPh ₃ 2	Ph ² PPh ₃ F-P ¹ -Rh-F Ph ³ PPh ₃ 3	Ph ² PPh ₃ F-P ¹ -Rh-F-H-F Ph ³ PPh ₃ 6
Geometry Parameter, Å or deg.				
Rh-F	2.070(2)		2.038(2)	2.082(1)
Rh-P ¹	2.193(1)	2.153(1)	2.1338(8)	2.1342(5)
Rh-P ²	2.325(1)	2.317(1)	2.2921(7)	2.3178(5)
Rh-P ³	2.325(1)	2.334(1)	2.3221(8)	2.3423(5)
P ¹ -F		1.614(2)	1.616(2)	1.609(1)
F-Rh-P ¹	166.90(6)		176.45(4)	176.77(3)
F-Rh-P ³	86.50(7)		79.68(5)	81.51(3)
P ¹ -Rh-P ³	95.79(5)	91.46(4)	98.31(3)	95.64(2)
F-Rh-P ²	85.51(7)		89.79(5)	91.10(3)
P ¹ -Rh-P ²	96.21(5)	95.73(4)	92.50(3)	91.87(2)
P ² -Rh-P ³	159.71(4)	172.10(4)	167.90(2)	171.02(2)
Rh-Cl		2.396(1)		
P ¹ -Rh-Cl		176.13(4)		
P ³ -Rh-Cl		89.03(3)		
P ² -Rh-Cl		83.58(3)		

square-planar d⁸ complexes has been discussed in reviews^{1,7,25} and numerous experimental papers. For instance, the Pd–F bond in *trans*-[(Ph₃P)₂Pd(Ar)F] has been found³⁰ shorter, by ca. 0.035 Å, for Ar = 4-NO₂C₆H₄ than for Ar = Ph. Also, stable complexes of the type *trans*-[(*i*-Pr₃P)₂Rh(F)(L)] have been reported⁴¹ to form upon treatment of [(*i*-Pr₃P)₄Rh₂(μ-F)₂] with L = CO, CNR, PhC≡CPh, or CH₂=CH₂ but not with weaker π-acids Py or MeCN. Because in square-planar d⁸ transition metal fluorides π-donation from F to the empty d(x²-y²) orbital is symmetry forbidden, destabilizing filled/filled d_π-p_π M–F repulsion²⁵ can only be alleviated via back-donation from the filled d orbitals on M to the vacant antibonding orbital of a π-acidic ligand trans to F. Both push–pull interactions of the lone pairs on F with a π-acceptor trans to it through filled d-orbitals on the metal^{25,69} and electrostatic effects⁵ are believed to diminish the strength of the filled/filled repulsion and hence stabilize the M–F bond. In contrast with the different Rh–F bonds in **1** and **3**, the Rh–Cl bonds in Wilkinson’s catalyst (2.404(4) and 2.376(4) Å,⁶⁴ see Table 1) and in **2** (2.396(1) Å) are similar in length, indicating that the M–X filled/filled repulsion diminishes considerably when going from X = F to X = Cl.

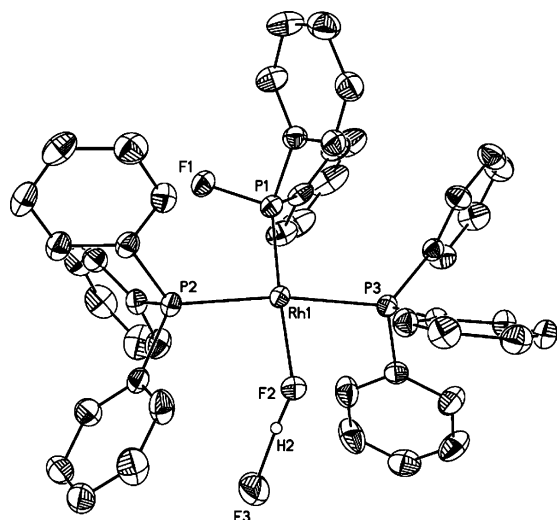


Figure 4. ORTEP drawing of **6** with thermal ellipsoids drawn to the 50% probability level and all H atoms, except for FHF, omitted for clarity.

(3) Complex **6** is a new member of the small family of transition metal complexes containing bifluoride as a ligand.^{27,28,31,38,41,46,52,70–79} All geometry parameters found for **6** and the analogous fluoride **3** are similar, except the Rh–F bond in **6** is elongated by ca. 0.04 Å, as a result of HF hydrogen bonding. Likewise, the M–F bonds in [(COD)Rh(PPh₃)(FHF)]⁵² and [(Ph₃P)₂Pd(Ph)(FHF)]⁷⁸ are longer than those in [(COD)-Rh(PPh₃)(F)]⁵² and [(Ph₃P)₂Pd(Ph)(F)]²⁷ respectively. The F···F distance (2.329 Å) and the F–F–Rh angle (135.6°) in **6** are within the range reported for other bifluoride complexes.

(4) All complexes **1**, **2**, **3**, and **6** exhibit CH···F interactions, contacts that are shorter than the sum of the van der Waals radii of fluorine (1.47 Å) and hydrogen (1.20 Å), a common phenomenon in organometallic fluorine chemistry.⁸⁰ It is noteworthy that such short CH···F contacts are also observed for the fluorine atoms bonded to phosphorus in the Ph₂PF ligand of **2**, **3**, and **6**. Because in a recent publication,³⁴ CH···F contacts in [(*i*-Pr₃P)₄Rh₂(μ-F)₂] were overlooked,⁸¹ an ORTEP showing these contacts is presented in Figure 5.

Basic Characteristics of the Thermal Decomposition of 1. Detection, Isolation, and Full Characterization of the Intermediate, *cis*-[(Ph₃P)₂Rh(Ph)(Ph₂PF)], 5. The thermal

- (67) For a review, see: Dias, P. B.; Minas de Piedade, M. E.; Martinho Simões, J. A. *Coord. Chem. Rev.* **1994**, 135/136, 737.
 (68) (a) Moloy, K. G.; Petersen, J. L. *J. Am. Chem. Soc.* **1995**, 117, 7696. (b) Huang, J.; Haar, C. M.; Nolan, S. P.; Marshall, W. J.; Moloy, K. G. *J. Am. Chem. Soc.* **1998**, 120, 7806.
 (69) Mayer, J. M. *Comments Inorg. Chem.* **1988**, 8, 125.
 (70) Coulson, D. R. *J. Am. Chem. Soc.* **1976**, 98, 3111.
 (71) Roesky, H. W.; Sotoodeh, M.; Xu, Y. M.; Schrupf, F.; Noltemeyer, M. *Z. Anorg. Allg. Chem.* **1990**, 580, 131.
 (72) Hintermann, S.; Pregosin, P. S.; Rüegger, H. *J. Organomet. Chem.* **1992**, 435, 225.
 (73) Whittlesey, M. K.; Perutz, R. N.; Greener, B.; Moore, M. H. *Chem. Commun.* **1997**, 187.
 (74) Murphy, V. J.; Hascall, T.; Chen, J. Y.; Parkin, G. *J. Am. Chem. Soc.* **1996**, 118, 7428. Murphy, V. J.; Rabinovich, D.; Hascall, T.; Klooster, W. T.; Koetzle, T. F.; Parkin, G. *J. Am. Chem. Soc.* **1998**, 120, 4372.
 (75) Holzbock, J.; Sawodny, W.; Walz, L. *Z. Kristallogr.* **1997**, 212, 115. Bentrup, U.; Harms, K.; Massa, W.; Pebler, J. *Solid State Sci.* **2000**, 2, 373.
 (76) Braun, T.; Foxon, S. P.; Perutz, R. N.; Walton, P. H. *Angew. Chem., Int. Ed.* **1999**, 38, 3326.
 (77) Jasim, N. A.; Perutz, R. N. *J. Am. Chem. Soc.* **2000**, 122, 8685.
 (78) Roe, D. C.; Marshall, W. J.; Davidson, F.; Soper, P. D.; Grushin, V. V. *Organometallics* **2000**, 19, 4575.
 (79) Archibald, S. J.; Braun, T.; Gaunt, J. A.; Hobson, J. E.; Perutz, R. N. *Dalton Trans.* **2000**, 2013.
 (80) Brammer, L.; Bruton, E. A.; Sherwood, P. *Cryst. Growth Des.* **2001**, 1, 277.

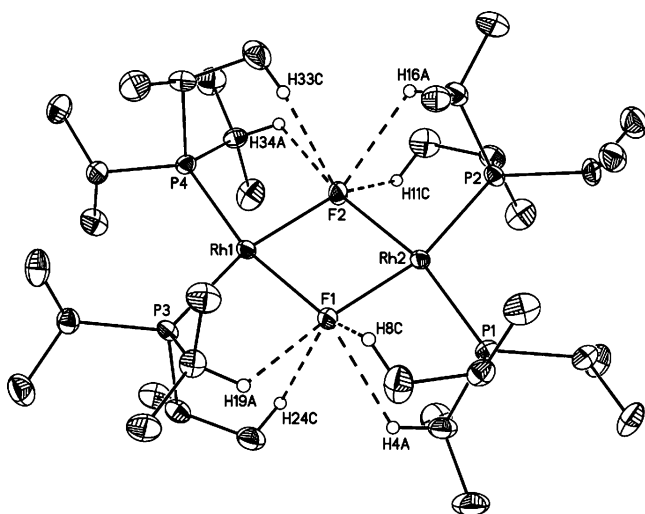


Figure 5. ORTEP drawing of $[(i\text{-Pr}_3\text{P})_4\text{Rh}_2(\mu\text{-F})_2]$ showing $\text{CH}\cdots\text{F}$ contacts that were previously missed.^{34,81} All other H atoms are omitted for clarity. Thermal ellipsoids are drawn to the 50% probability level.

decomposition of **1** to **3** and **4** was chosen for studies aimed at understanding the mechanism of the P–C bond cleavage and P–F bond formation (eq 3). In a series of preliminary studies by ^{19}F and ^{31}P NMR, some important observations were made, as follows.

(1) The rate of reactions 2 and 3 was not influenced by free PPh_3 (up to 25 equiv), which was deliberately added to the reaction mixtures. This observation was in accord with the enhanced thermal stability of $[(\text{PPh}_3)_4\text{Rh}_2(\mu\text{-F})_2]$, which forms upon spontaneous dissociation of PPh_3 from **1** in solution (eq 5). In sharp contrast to >90% conversion of **1** after 3 h at 80 °C in benzene, $[(\text{PPh}_3)_4\text{Rh}_2(\mu\text{-F})_2]$ did not decompose under these conditions. This result also indicated that no phosphine pre-dissociation from **1** was required for reactions 2 and 3 to occur.

(2) In a series of separate experiments, it was found that the cyclometalation of $[(\text{Ph}_3\text{P})_3\text{RhPh}]$, **B**,⁵⁸ to **4** (Scheme 1) was decelerated by extra PPh_3 . The ambient temperature ^{31}P NMR spectrum of $[(\text{Ph}_3\text{P})_3\text{RhPh}]$, with or without extra PPh_3 , displayed an unsymmetrical doublet-like looking signal at 32.7 ppm ($J = 162.4$ Hz). The cyclometalated product **4** exhibited three resonances with the chemical shifts and coupling constants being in full accord with the literature data.⁶⁶ In a freshly prepared benzene solution devoid of added PPh_3 , **B** underwent ca. 10% conversion to **4** after just 20 min at room temperature, as indicated by ^{31}P NMR. However, in the presence of 2 equiv of extra PPh_3 , **B** was much less prone to cyclometalation, and only trace amounts of **4** (<5%) were formed after 3 days. At 80 °C, **B** transformed to **4** rapidly, even in the presence of a 10-fold excess of PPh_3 .

(3) In the very slow decomposition reaction of **1** at a low temperature (25–40 °C), the appearance and subsequent disappearance of **B** was observed. Even more pronounced was an intermediacy of another species, which displayed signals with a large coupling constant $J_{\text{P-F}} = 869$ Hz in both the ^{19}F and

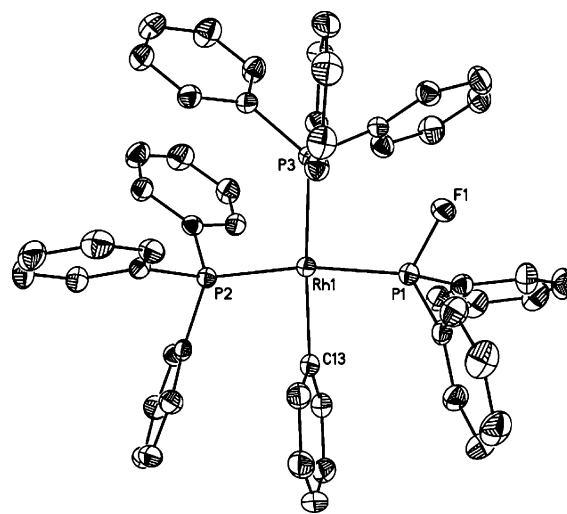


Figure 6. ORTEP drawing of $5 \cdot 2\text{C}_6\text{H}_6$ with thermal ellipsoids drawn to the 50% probability level. The solvent molecules and all H atoms are omitted for clarity. Selected bond distances (Å) and bond angles (deg): Rh(1)–C(13) 2.070(2); Rh(1)–P(1) 2.2192(5); Rh(1)–P(3) 2.3183(5); Rh(1)–P(2) 2.3189(5); P(1)–F(1) 1.604(1); C(13)–Rh(1)–P(1) 82.78(5); C(13)–Rh(1)–P(3) 170.55(5); P(1)–Rh(1)–P(3) 91.42(2); C(13)–Rh(1)–P(2) 88.03(5); P(1)–Rh(1)–P(2) 168.67(2); P(3)–Rh(1)–P(2) 98.53(2); F(1)–P(1)–C(1) 98.40(8).

the ^{31}P NMR spectra, pointing to P–F bond formation upon thermolysis of **1** at 40–80 °C.

Having made these observations, we attempted isolation of this intermediate. Preliminary NMR kinetic studies were conducted on the thermal decomposition of **1** in the presence of extra PPh_3 . The latter was used (i) to shift equilibrium 5 to the reactive **1**, thus minimizing the presence of phosphine-deficient, much more thermally stable $[(\text{PPh}_3)_4\text{Rh}_2(\mu\text{-F})_2]$, and (ii) to slow the irreversible cyclometalation of **B** (Scheme 1), which would drive all of the equilibria to the final products, **3** and **4**. It was found that the highest concentration of the intermediate could be reached after **1** and PPh_3 (4 equiv) were heated in benzene at 70 °C for 1 h. These conditions were then used to scale-up the reaction for isolation of the intermediate. It was found that unlike the starting material (**1**) and the product (**3**), the intermediate was soluble in ether, albeit only in the presence of extra PPh_3 . This observation led to the development of an efficient procedure for isolation of the pure intermediate in 19–29% yield.

Single-crystal X-ray diffraction revealed the structure of the intermediate as *cis*- $[(\text{Ph}_3\text{P})_2\text{Rh}(\text{Ph})(\text{Ph}_2\text{PF})]$ (**5**; Figure 6).⁸² This product of direct positional exchange between the fluorine and a phenyl in **1** was the “missing link” of the proposed mechanistic model, as shown in Scheme 1. Computer simulation of an *ABMX*Y spin system (A, B, and M = ^{31}P ; X = ^{19}F ; Y = ^{103}Rh) produced patterns that are in excellent agreement with the experimental ^{19}F and ^{31}P NMR spectra of **5** (Figures 7 and 8). A weak broadened doublet at –132 ppm with $J_{\text{P-F}} = \text{ca. } 860$ Hz was commonly observed in the ^{19}F NMR spectrum of purified samples of **5** (Figure 7). Because of the low content (ca. 5% of **5**), no attempt was made to characterize this species. We carefully propose that the weak doublet might be from the *trans* isomer of **5** or perhaps from a dimeric species such as $[(\text{PPh}_3)_2(\text{PPh}_2\text{F})_2\text{Rh}_2(\mu\text{-F})_2]$.

(81) W.J.M. and V.V.G. are thankful to Professor Santiago Alvarez and Dr. Gabriel Aullón for bringing this to our attention. Previously, intramolecular $\text{CH}\cdots\text{F}$ contacts in $[(i\text{-Pr}_3\text{P})_4\text{Rh}_2(\mu\text{-F})_2]$ were missed³⁴ using the Cambridge Mercury program, version 1.3. This is mentioned as a cautionary note that clicking on “Short Contact < (sum of vdw radii)” does not include intramolecular contacts unless they are more explicitly defined using the sub-menu “Define short contacts”.

(82) Two solvates of **5**, *cis*- $[(\text{Ph}_3\text{P})_2\text{Rh}(\text{Ph})(\text{Ph}_2\text{PF})] \cdot \text{Et}_2\text{O}$ and *cis*- $[(\text{Ph}_3\text{P})_2\text{Rh}(\text{Ph})(\text{Ph}_2\text{PF})] \cdot 2\text{C}_6\text{H}_6$, were studied by single-crystal X-ray diffraction.

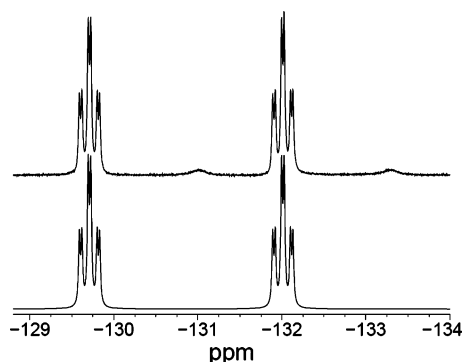
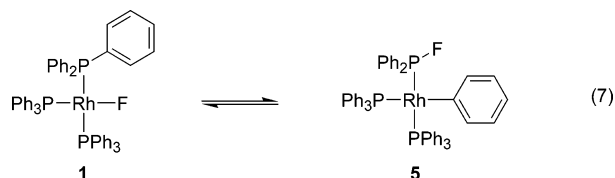


Figure 7. Experimental (top) and simulated (bottom) ^{19}F NMR spectra of **5** in benzene (20 °C). The simulations lead to the following parameters characterizing the *ABMXY* spin system: **A**, PPh_3 trans to PFPh_2 , 36.6 ppm, $\text{cis-}^2J_{\text{P-P}} = -29.1$ Hz, $\text{trans-}^2J_{\text{P-P}} = 383.1$ Hz, $\text{trans-}^3J_{\text{P-F}} = 39.4$ Hz, $^1J_{\text{P-Rh}} = -154.8$ Hz; **B**, PPh_3 cis to PFPh_2 , 37.9 ppm, $\text{cis-}^2J_{\text{P-P}} = -40.3$ Hz, $\text{cis-}^3J_{\text{P-F}} = 41.6$ Hz, $^1J_{\text{P-Rh}} = -122.0$ Hz; **M**, PFPh_2 , 171.9 ppm, $^1J_{\text{P-F}} = 868.6$ Hz, $^1J_{\text{P-Rh}} = -214.6$ Hz; **X**, PFPh_2 , -131.0 ppm, $^2J_{\text{F-Rh}} = 10.0$ Hz.

The F–Ph Rearrangement of 1 to 5 Is Reversible. Kinetic Studies of the F/Ph Exchange. It was found that **5** readily decomposes in benzene at 80 °C to give cleanly **3** and **4**, just as if **1** rather than **5** were being used for the reaction (eq 3). When the thermal decomposition of **5** at 40–60 °C was monitored by ^{19}F and ^{31}P NMR, the intermediate formation of **1** was observed. These experiments indicated that the F/Ph exchange reaction of **1** to produce **5** is reversible (eq 7). To gain insight into the mechanism of this Ph/F rearrangement, a kinetic study of reaction 7 was carried out, with the equilibrium being approached from both sides.



As can be seen from Scheme 2, two side processes could complicate the kinetic measurements (^{19}F NMR) of the Ph/F exchange (eq 7), (i) the dimerization of **1** to give $[(\text{PPh}_3)_4\text{Rh}_2(\mu\text{-F})_2]$ and (ii) ligand exchange between **1** and **5** to produce **3**

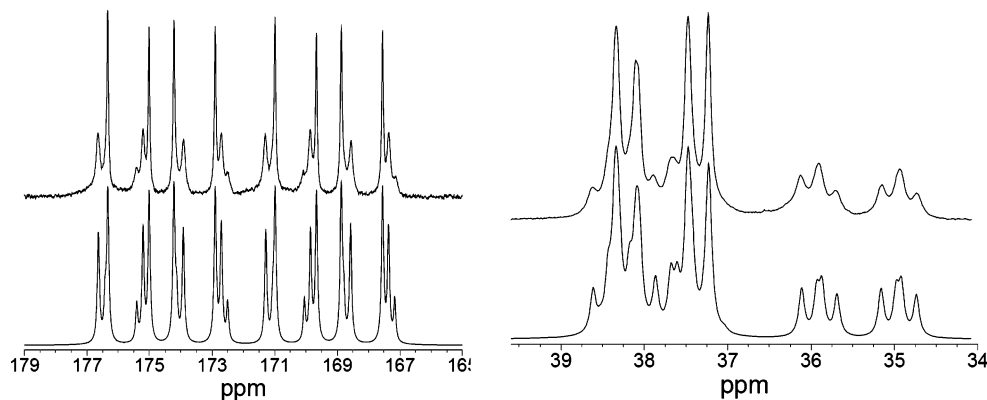
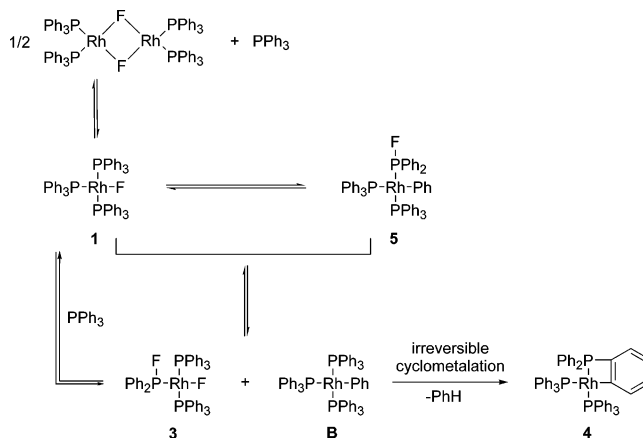


Figure 8. Experimental (top) and simulated (bottom) ^{31}P NMR spectra of **5** in benzene (20 °C). The simulations lead to the following parameters characterizing the *ABMXY* spin system: **A**, PPh_3 trans to PFPh_2 , 36.6 ppm, $\text{cis-}^2J_{\text{P-P}} = -29.1$ Hz, $\text{trans-}^2J_{\text{P-P}} = 383.1$ Hz, $\text{trans-}^3J_{\text{P-F}} = 39.4$ Hz, $^1J_{\text{P-Rh}} = -154.8$ Hz; **B**, PPh_3 cis to PFPh_2 , 37.9 ppm, $\text{cis-}^2J_{\text{P-P}} = -40.3$ Hz, $\text{cis-}^3J_{\text{P-F}} = 41.6$ Hz, $^1J_{\text{P-Rh}} = -122.0$ Hz; **M**, PFPh_2 , 171.9 ppm, $^1J_{\text{P-F}} = 868.6$ Hz, $^1J_{\text{P-Rh}} = -214.6$ Hz; **X**, PFPh_2 , -131.0 ppm, $^2J_{\text{F-Rh}} = 10.0$ Hz.

and **B**, with the latter undergoing the facile irreversible cyclometalation to **4**. Preliminary observations regarding the thermolysis kinetics of **1** indicated that varying the concentration of PPh_3 did not have a significant impact on the rate (see above). Likewise, dilution of the starting solution by approximately a factor of 3 did not lead to a marked decrease in the observed reaction rate. Therefore, to suppress the formation of the dimer $[(\text{PPh}_3)_4\text{Rh}_2(\mu\text{-F})_2]$, the kinetic experiments were run in the presence of a 12-fold excess of extra PPh_3 . In this way, the equilibrium between **1** and the dimer (eq 5) was efficiently shifted toward **1** without influencing the rate of exchange under study (eq 7 and Scheme 2). Also, it was reasoned that because the formation of **3** and **B** via ligand exchange between **1** and **5** is second order, the fluorine transfer step could be isolated kinetically by using as low a concentration of **1** or **5** as was practicable for kinetic observations. Indeed, it was established that for $[\mathbf{1}]$ or $[\mathbf{5}] = 4 \times 10^{-3}$ mol dm^{-3} reaction 7 was amenable to a kinetic study by ^{19}F NMR. At this concentration, the undesired bimolecular P ligand exchange processes leading to **3** and **B** were slow enough to remain kinetically insignificant in the 30–60 °C temperature range.

Scheme 2



The results of one kinetic run, at 40 °C, are presented in Figure 9, showing the approach to equilibrium starting from **1** (A) and from **5** (B). Analogous results of the other runs at 30, 50, 60, and 70 °C can be found in the Supporting Information.

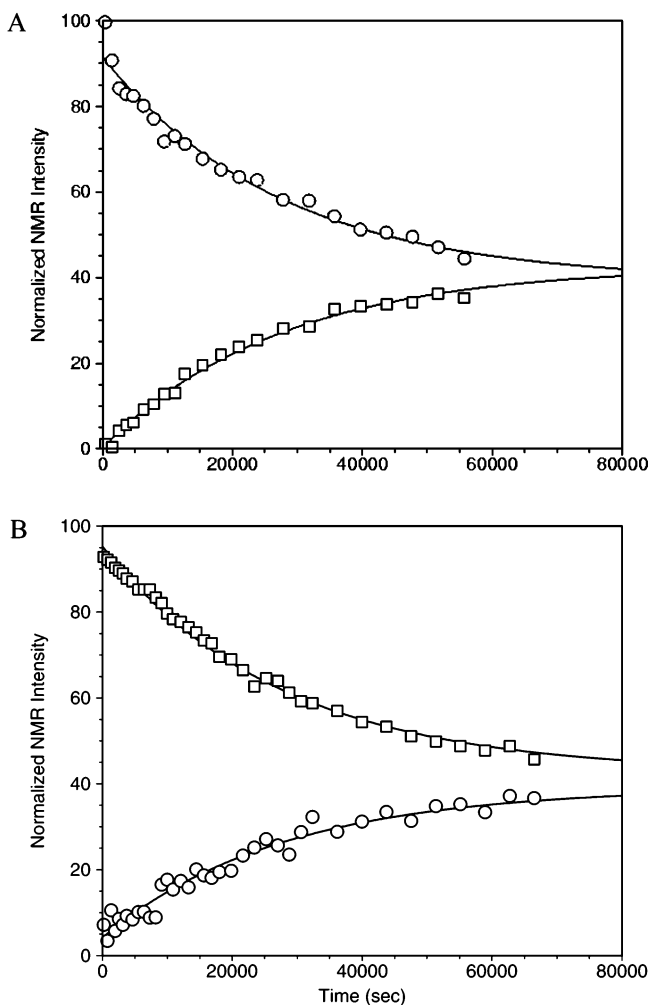


Figure 9. (A) The approach to equilibrium at 40 °C starting from **1** (○), and (B) starting from **5** (□).

The approach to equilibrium was modeled according to standard kinetic equations.⁸³

$$A(t) = (A_{\text{init}} - A_{\text{eqm}}) \exp(-(k_1 + k_{-1})t) + A_{\text{eqm}}$$

$$B(t) = (B_{\text{init}} - B_{\text{eqm}}) \exp(-(k_1 + k_{-1})t) + B_{\text{eqm}}$$

where $A(t)$ and $B(t)$ are the observed intensities at time t , the subscripts “init” and “eqm” refer to initial and equilibrium intensities, k_1 is the forward rate constant (**1** going to **5**), and k_{-1} is the reverse rate constant. The combined data sets were subjected to nonlinear least-squares optimization using initial intensities as parameters that were necessarily distinct between the two experiments, along with the single best-fitting rate constant ($k_1 + k_{-1}$) and equilibrium intensities consistent with the entire data set. The best-fitting parameters were used to obtain the smooth curves in Figure 9 and other kinetic plots (see Supporting Information), and the rate constant of interest (k_1) was obtained from the equilibrium intensities, $k_1 = (k_1 + k_{-1}) / (1 + A_{\text{eqm}}/B_{\text{eqm}})$. At 30 °C, only the reverse reaction could be analyzed due to the lack of solubility of **1**. This, however, was not a problem for the reverse process as **5** is much more easily soluble in benzene than **1**. At 70 °C, we were clearly at

the limit of our ability to obtain meaningful data. The trend in the values obtained for A_{eqm} and B_{eqm} in the range 30–60 °C is for K_{eq} to decrease slightly from 0.9 to 0.6, whereas at 70 °C the estimated parameters lead to K_{eq} closer to 1.2. The data at 70 °C are therefore somewhat suspect, although the rate estimate at this temperature does not appear to have a significant impact on the determination of the activation parameters.

Table 4. Estimated Rate Constants for the Conversion of **1** to **5** as a Function of Temperature

temp (°C)	k_1 (s^{-1} , $\times 10^5$)
30	0.51
40	1.90
50	5.38
60	14.7
70	43.6

The rate constants obtained in a benzene–benzene- d_6 mixture by this approach are presented in Table 4. The data in Table 4 are well described by the transition state treatment of the temperature dependence of reaction rate constants as judged by the linearity of the corresponding Eyring plot in Figure 10. The activation enthalpy (ΔH^\ddagger) and entropy (ΔS^\ddagger) were determined by direct nonlinear least-squares fitting of these parameters to the Eyring equation ($k_1 = (k_B T/h) \exp(\Delta S^\ddagger/R) \exp(-\Delta H^\ddagger/RT)$) using the temperature and rate constant data in Table 4. This fitting procedure gave the parameter estimates $\Delta H^\ddagger = 22.0 \pm 1.2$ kcal mol $^{-1}$ and $\Delta S^\ddagger = -10.0 \pm 3.7$ eu (the corresponding Arrhenius parameters are $E_a = 22.7 \pm 1.2$ kcal mol $^{-1}$ and $\log(A/s^{-1}) = 11.1 \pm 0.8$). The stated uncertainties represent 95% confidence limits and were obtained using an estimated error in the rate constants of 10% and an estimated error in temperature of 2 °C. When the rate constant at 70 °C was omitted from the analysis (see above), the estimated activation parameters were $\Delta H^\ddagger = 21.8 \pm 2.6$ kcal mol $^{-1}$ and $\Delta S^\ddagger = -10.8 \pm 8.0$ eu.

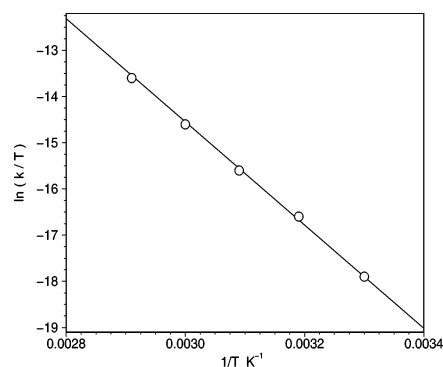


Figure 10. Eyring plot for the rate data presented in Table 4.

Solvent Effects on the F/Ph Rearrangement. In view of the possibility of solvent participation in the reaction, the reaction of **1** at 60 °C was repeated in THF- d_8 and led to a rate constant of $19.1 \times 10^{-5} s^{-1}$ (vs $14.7 \times 10^{-5} s^{-1}$ in benzene). Hence, in this case the reaction was not strongly influenced by solvent.

A series of semiquantitative studies indicated that in benzene–acetonitrile (78:22 by volume) and in benzene–DMSO (78:22 by volume), the reaction of **5** in the presence of PPh_3 to **1** was faster. Moreover, both MeCN and DMSO promoted phosphine ligand exchange (Scheme 2), the secondary processes leading

(83) Cox, B. G. *Modern Liquid-Phase Kinetics*; Oxford University Press: Oxford, UK, 1994.

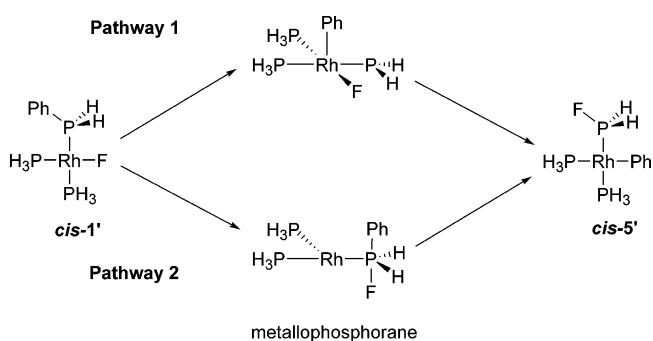
to $[(\text{Ph}_2\text{PF})(\text{Ph}_3\text{P})_2\text{RhF}]$ (**3**) and $[(\text{Ph}_3\text{P})_3\text{RhPh}]$ (**B**). The latter did not undergo cyclometalation (^{31}P NMR) because the reactions were run at a low temperature (25–45 °C) in the presence of a large excess of PPh_3 . The reaction of **1** to **5** was not observed in these solvent mixtures. A precise quantitative kinetic study in benzene–MeCN or benzene–DMSO could not be carried out due to the facilitated secondary processes, that is, P-ligand exchange (see above). When nitrobenzene was used instead of MeCN or DMSO, the reaction of **1** to **5** was slower than in pure benzene (by approximately a factor of 2), and the reaction of **5** to **1** was strongly accelerated, giving ca. 80% conversion at >90% selectivity to **1** versus <5% conversion without PhNO_2 . Unlike MeCN and DMSO, nitrobenzene did not promote any secondary ligand exchange processes at all.

The solvent effects observed were analyzed against the dielectric constant ϵ ⁸⁴ and Gutmann's donor and acceptor numbers⁸⁵ of the solvents (benzene, $\epsilon = 2.28$, DN = 0.1, AN = 8.2; THF, $\epsilon = 7.52$, DN = 20.0, AN = 8.0; MeCN, $\epsilon = 36.64$, DN = 14.1, AN = 19.3; DMSO, $\epsilon = 47.24$, DN = 29.8, AN = 19.3; PhNO_2 , $\epsilon = 35.6$, DN = 4.4, AN = 14.8). The reaction occurred at approximately the same rate in benzene and in slightly more polar but much more coordinating THF. All three highly polar solvents (MeCN, DMSO, and PhNO_2) accelerated the reaction of **5** to **1** and slowed the reverse process. Of these three polar solvents, the ones with higher donor numbers (MeCN and DMSO) also promoted the secondary P-ligand exchange processes, whereas poorly donating nitrobenzene did not. In addition to the polarity and denticity factors, the solvent's ability to form a hydrogen bond to the fluoride on Rh may also need to be taken into consideration, as MeCN and DMSO are better H-bond donors than benzene, nitrobenzene, and THF.

Theoretical Studies on the F/Ph Rearrangement of 1 to Give 5. We have employed density functional calculations to study F/Ph exchange in **1** using simplified models of the type $[(\text{PH}_3)_2(\text{PH}_2\text{Ph})\text{RhF}]$, **1'**. Two general mechanistic possibilities were considered that differ in the order of transfer of the Ph and F groups to and from the metal (Scheme 3). Pathway 1 proceeds via Ph group transfer from phosphine to Rh in what is formally an oxidative addition step. The Rh-phosphide intermediate can then undergo P–F bond-forming reductive elimination to produce $[(\text{PH}_3)_2(\text{PH}_2\text{F})\text{RhPh}]$, **5'**. In principle, Ph group transfer may occur from a phosphine either cis to F (**cis-1'**, as shown in Scheme 3) or from a site trans to F (**trans-1'**). Pathway 2 is characterized by an initial transfer of F from Rh to phosphine to form a metallophosphorane, from which Ph can transfer back to Rh to complete the F/Ph exchange process. The nature of this metallophosphorane necessitates that it will originate from **cis-1'**. In the following, it will be useful to consider metallophosphoranes formally as complexes between an anionic $[\text{PH}_2\text{FPh}]^-$ phosphoranide ligand and a Rh(I) metal center.

Metallophosphoranes⁸⁶ similar to that in Scheme 3 have been proposed as intermediates in the fluoride-promoted disproportionation of Pd(II) and Pt(II) phosphine complexes,⁸⁷ and one

Scheme 3



of us has identified computationally a metallophosphorane formed by methoxide transfer from Pt to phosphine as a low energy intermediate in the isomerization processes of $[(\text{H}_2\text{PCH}_2\text{CH}_2\text{PH}_2)(\text{CO})\text{Pt}(\text{Me})(\text{OMe})]$ model systems.⁸⁸ Moreover, the transfer of an aryl group from a phosphoranide ligand to an iridium metal center has also been reported.⁸⁹ Thus, there is precedent for both type of processes involved in pathway 2, the transfer of a hard ligand, such as fluoride, from metal to phosphine and the transformation of a metallophosphorane into a metal-phosphine/aryl complex.

Computed profiles for F/Ph exchange via pathway 1 are shown in Figures 11 (for **cis-1'**, pathway 1a) and 12 (for **trans-1'**, pathway 1b). Figure 11 also includes a comparison of the computed geometries of **cis-1'** and **cis-5'** with those determined crystallographically for **1** and **5**. The computed metal–ligand distances are well reproduced, in particular the shortening of the Rh–P bond trans to F and the Rh–PH₂F distance in **cis-5'**, where the latter is ca. 0.1 Å shorter than the Rh–PH₃ bonds. The Rh–F distance in **cis-1'** is somewhat too short in our calculations, probably due to the simplification of the phosphine ligands in our model. Indeed, in a second form of **cis-1'** in which a different orientation of the PH₂Ph ligand allows a short *ortho*-C–H...F distance of 2.108 Å to develop, a slightly longer Rh–F bond is computed (2.022 vs 2.005 Å), suggesting that such C–H...F contacts can lengthen metal–fluoride bonds. Overall the product of F/Ph exchange, **cis-5'**, is computed to be 2.3 kcal/mol less stable than the model reactant **cis-1'**, a trend that is consistent with the equilibrium lying slightly toward **1** experimentally (25 °C, benzene).

The first step in pathway 1a, transfer of Ph from phosphorus to Rh, proceeds with a dramatic shortening of the Rh...C(ipsos) distance from ca. 3.6 Å in **cis-1'** to only 2.22 Å in **TS_{cis-1'-II}**. This has the effect of pushing the {PH₂} moiety out of the metal coordination plane with the result that the phosphide ligand eventually moves into the axial position in the Rh(III) intermediate (**II**, $E = +10.4$ kcal/mol). The activation barrier for P–C bond activation is computed to be 24.7 kcal/mol, and during this process the phenyl ring adopts the perpendicular orientation predicted from extended Hückel calculations.⁹⁰ To our knowledge, this is the first time that the activation of a P–aryl bond by a transition metal center has been studied using high-level calculations.⁹¹ Interestingly, this process does not correspond to a simple Ph group transfer from phosphorus to metal, as this would be expected to place Ph in the axial position in

(84) Lide, D. R. *Handbook of Organic Solvents*; CRC Press: Boca Raton, FL, 1995.

(85) Gutmann, V. *Electrochim. Acta* **1976**, *21*, 661.

(86) For a review of metallophosphoranes, see: Nakazawa, H.; Kubo, K.; Miyoshi, K. *Bull. Chem. Soc. Jpn.* **2001**, *74*, 2255.

(87) Mason, M. R.; Verkade, J. G. *Organometallics* **1992**, *11*, 2212.

(88) Macgregor, S. A.; Neave, G. W. *Organometallics* **2004**, *23*, 891.

(89) Kajiyama, K.; Nakamoto, A.; Miyazawa, S.; Miyamoto, T. K. *Chem. Lett.* **2003**, *32*, 332.

(90) Ortiz, J. V.; Haviyas, Z.; Hoffmann, R. *Helv. Chim. Acta* **1984**, *67*, 1.

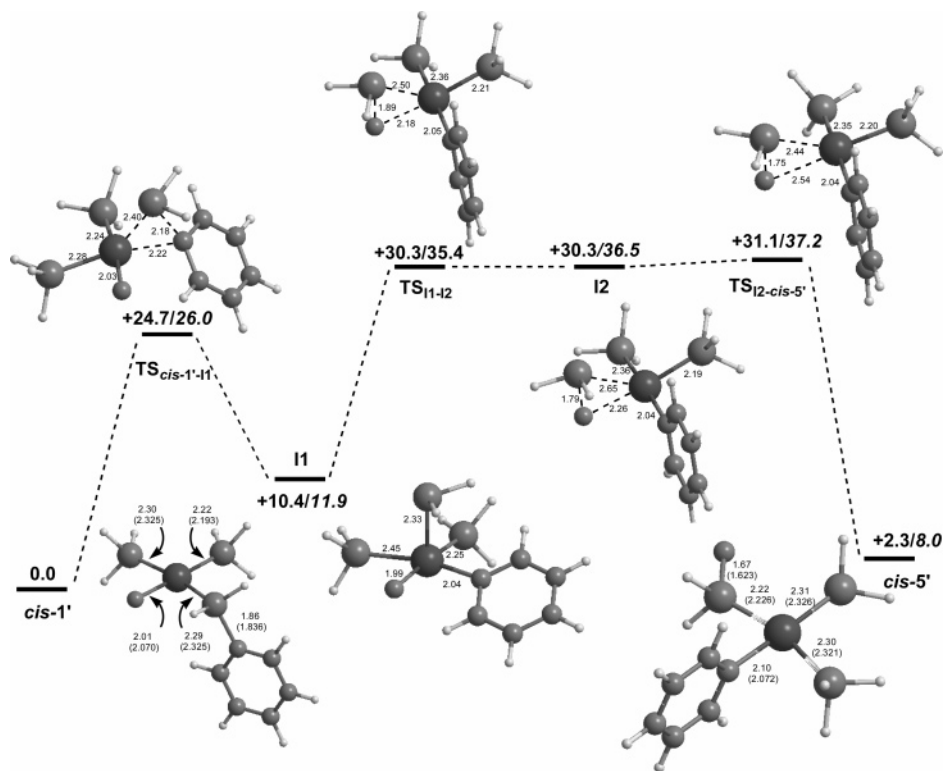


Figure 11. Computed reaction profile (kcal/mol) for pathway 1a in vacuo and in DMSO ($\epsilon = 46.7$; italicized) with selected distances in angstroms. For *cis-1'* and *cis-5'*, comparisons with the experimental distances from **1** and **5** are given in parentheses. In the drawing of *cis-1'*, the value of 1.836 Å shown in parentheses is the average of the experimental P–C distances for the *cis* PPh_3 ligands of **1**.

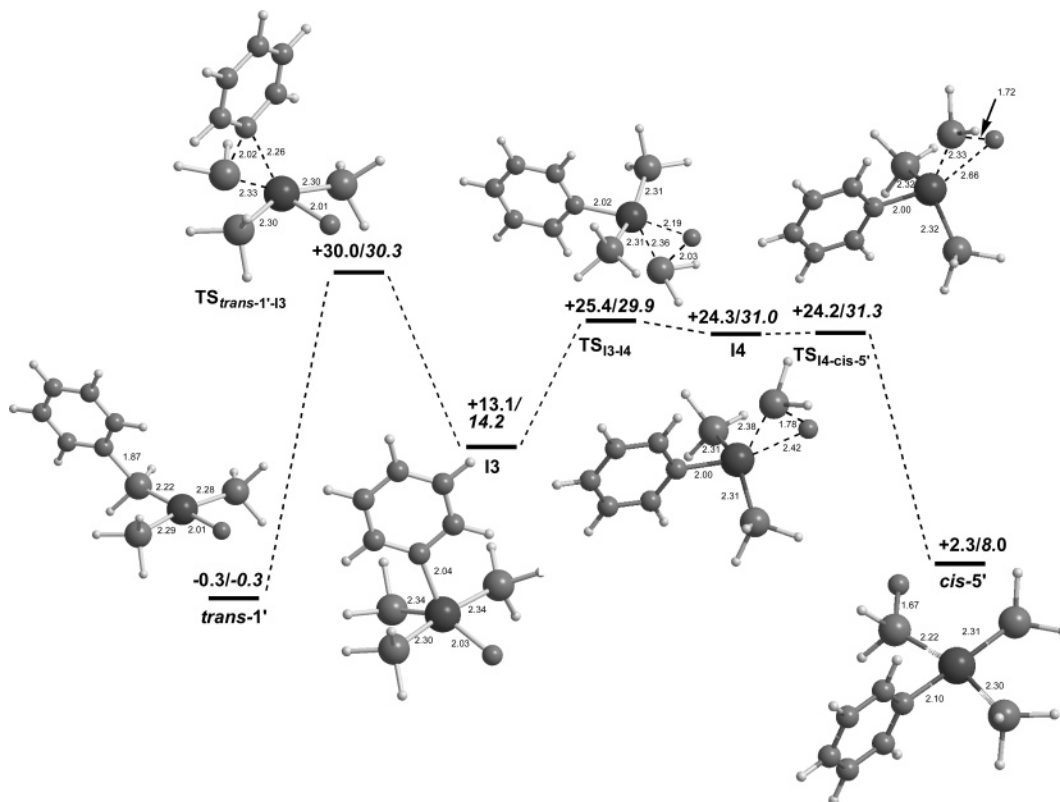


Figure 12. Computed reaction profile (kcal/mol) for pathway 1b in vacuo and in DMSO ($\epsilon = 46.7$; italicized) with selected distances in angstroms.

II. Instead, P–C activation appears to involve extrusion of the $\{\text{PH}_2\}$ moiety; the reverse process from **II** to *cis-1'* could certainly be viewed as PH_2 insertion into the Rh–Ph bond.

The geometry of **II**, with PH_2 *cis* to F, is set up for P–F bond-forming reductive elimination, and a transition state corresponding to this process was located ($\text{TS}_{\text{II}-\text{I2}}$, $E = +30.3$

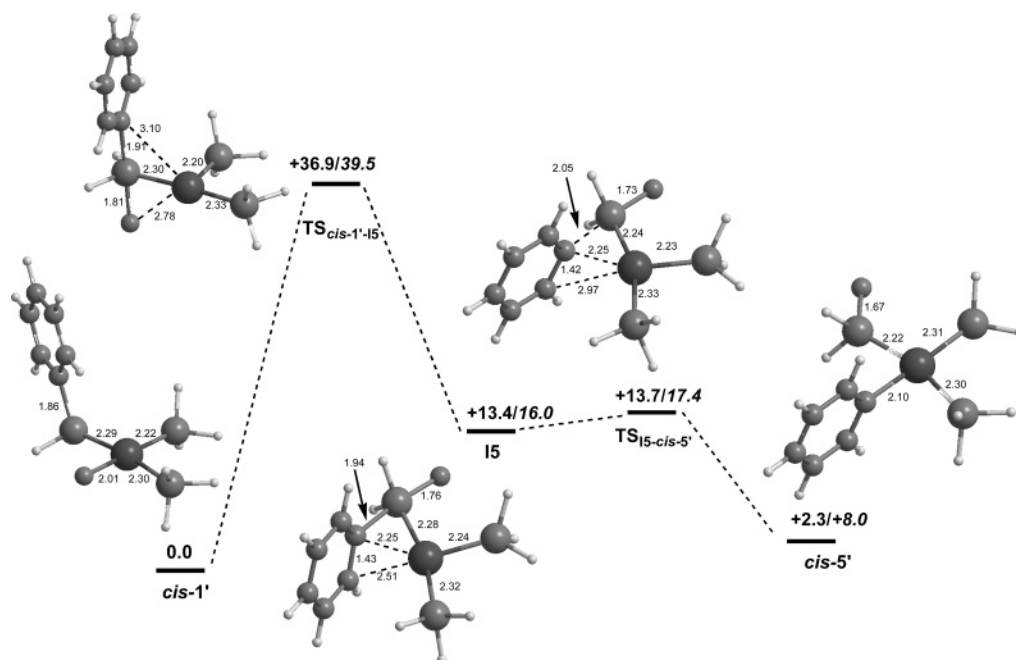


Figure 13. Computed reaction profile (kcal/mol) for pathway 2a in vacuo and in DMSO ($\epsilon = 46.7$; italicized) with selected distances in angstroms.

kcal/mol). Unexpectedly, however, this transition state led to a new intermediate (**I2**, $E = +30.3$ kcal/mol),⁹² where the PH_2F ligand appears to bind in an agostic fashion to the metal center via the P–F bond ($\text{P}\cdots\text{F} = 1.79$ Å). A transition state to complete the P–F bond formation process was then located by lengthening the $\text{Rh}\cdots\text{F}$ distance ($\text{TS}_{12-cis-5'}$, $E = +31.1$ kcal/mol), and this was found to lead to the model F/Ph exchange product, *cis*-5'. Intermediate **I2** therefore exists as a very shallow minimum, but IRC calculations do confirm that both TS_{11-12} and $\text{TS}_{12-cis-5'}$ link to this structure. Overall, $\text{TS}_{12-cis-5'}$ is the highest point along the pathway for conversion of *cis*-1' to *cis*-5' via pathway 1a, corresponding to a total computed activation barrier of 31.1 kcal/mol.

In pathway 1b, Ph group transfer from *trans*-1' ($E = -0.3$ kcal/mol) proceeds through transition state $\text{TS}_{\text{trans-1'-13}}$ ($E = +30.0$) to give a new five-coordinate intermediate **I3** ($E = +13.1$). In sharp contrast to pathway 1a, P–C bond cleavage in this case does correspond to a Ph group transfer with the $\{\text{PH}_2\}$ moiety barely moving out of the metal coordination plane. **I3** exhibits a distorted trigonal bipyramidal Y-shaped geometry with axial PH_3 ligands and large F–Rh–C(ipso) and F–Rh– PH_2 angles of 133° and 139° , respectively. Such a structure is typical of five-coordinate d^6 metal centers featuring a π -donor ligand.⁹³ P–F bond formation from **I3** therefore requires a significant movement of the PH_2 ligand, and the F–Rh– PH_2 angle narrows accordingly to a value of 53° in TS_{13-14} ($E = +25.4$ kcal/mol). In a similar way to TS_{11-12} in pathway 1a, TS_{13-14} does not lead directly to the final product but instead to an η^2 -P,F-agostic intermediate (**I4**, $E = +24.3$

kcal/mol), and a further transition state has to be located to complete the P–F bond formation process ($\text{TS}_{14-cis-5'}$, $E = +24.2$).⁹² The structure of $\text{TS}_{14-cis-5'}$ is rather unusual, however, being reminiscent of a trigonal bipyramid with one missing axial ligand. IRC and geometry optimization calculations beyond this transition state showed that $\text{TS}_{14-cis-5'}$ links to the F/Ph exchange product *cis*-5' and not, as might have been initially expected from the geometry of **I3**, to the alternative form, *trans*-5'. All attempts to locate a transition state linking **I4** directly to *trans*-5' failed, and converged instead on structures that ultimately would lead to *cis*-5'. Overall, the barrier associated with the conversion of *trans*-1' to *cis*-5' is +30.0 kcal/mol, slightly lower than that along pathway 1a, although in this case the highest point along the profile corresponds to the P–C activation rather than the P–F bond-forming step.

For pathway 2, two routes for F/Ph exchange via a metallophosphorane structure have been characterized, referred to in the following as pathways 2a and 2b. The computed profile for pathway 2a is shown in Figure 13. We initially searched for a metallophosphorane pathway by systematically decreasing the relevant $\text{P}\cdots\text{F}$ distance. When this led only to a steady increase in energy, we coupled this motion to rotation about the Rh– PH_2Ph bond, and this eventually allowed us to locate a metallophosphorane structure, however not as an intermediate but as a transition state ($\text{TS}_{cis-1'-15}$, $E = +36.9$ kcal/mol). The five-coordinate phosphorus center in this species exhibits a trigonal bipyramidal geometry, with the exchanging F and Ph in axial positions (angles at P: $\text{C}_{\text{ax}}\text{--P--Rh} = 94.3^\circ$; $\text{F}_{\text{ax}}\text{--P--Rh} = 84.0^\circ$; $\text{H}_{\text{eq}}\text{--P--Rh} = 119^\circ/130^\circ$). The Rh– PH_2FPh bond (2.30 Å) is similar in length to the Rh– PH_2Ph bond computed in *cis*-1', although the elongation of the trans Rh– PH_3 distance (to 2.33 Å from 2.30 Å in *cis*-1') suggests a slightly higher ligand trans influence for PH_2FPh as compared to PH_2Ph . IRC and geometry optimization calculations beyond $\text{TS}_{cis-1'-15}$ led to the new intermediate, **I5** ($E = +13.4$). This structure is formed by rotation around the Rh– PH_2FPh

(91) Hoffmann⁹⁰ reported a barrier of only 1.8 kcal/mol with EOMO calculations for Ph group transfer in a $[\text{PdH}_3(\text{PH}_2\text{Ph})]^-$ model. However, this figure is relative to a $[\text{PdH}_3(\text{PH}_2\text{Ph})]^-$ reactant in which the PH_2Ph ligand has a highly distorted geometry and so omits the reorganization energy associated with this distortion.

(92) The energy of **I2** is computed to be 0.3 kcal/mol more stable than that of TS_{11-12} before the inclusion of zero-point energy corrections. Similarly, **I4** is 0.2 kcal/mol more stable than $\text{TS}_{14-cis-5'}$ prior to this correction.

(93) Riehl, J.-F.; Jean, Y.; Eisenstein, O.; Péliissier, M. *Organometallics* **1992**, *11*, 729.

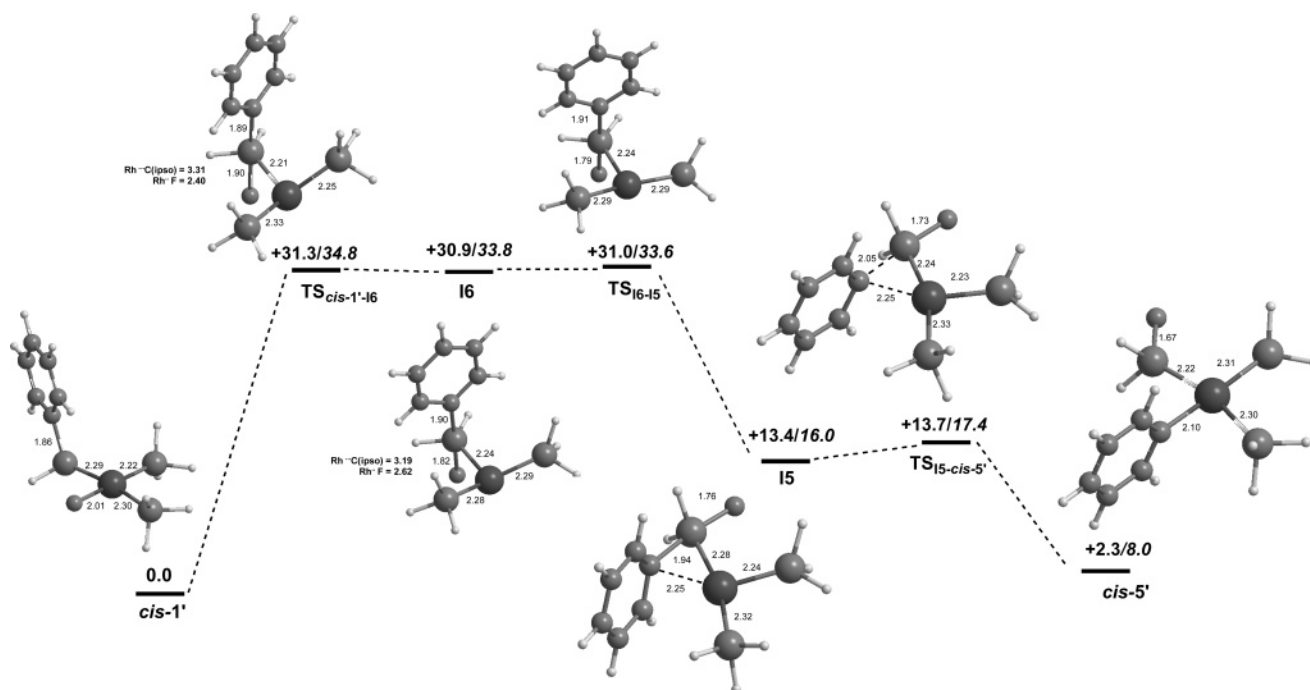


Figure 14. Computed reaction profile (kcal/mol) for pathway 2b in vacuo and in DMSO ($\epsilon = 46.7$; italicized) with selected distances in angstroms.

bond to bring the phenyl ring into proximity with the metal, allowing an interaction between Rh and the phenyl ring to be established ($\text{Rh}-\text{C}(\text{ipso}) = 2.25 \text{ \AA}$). The $\{\text{PH}_2\text{FPh}\}$ moiety is relatively unchanged in both **I5** and $\text{TS}_{\text{cis-1'-15}}$ with only a slight elongation of the P–C bond in the former. Intermediate **I5** could therefore be described as containing an η^2 -(P–C) phosphoranide ligand, similar to those observed with more strongly donating heteroatom substituents at phosphorus.⁹⁴ **I5**, however, represents only a shallow local minimum on the potential energy surface, and the subsequent full cleavage of the P–C bond occurs with a minimal activation barrier of 0.3 kcal/mol via $\text{TS}_{\text{I5-cis-5'}}$ ($E = +13.7$ kcal/mol). The overall activation barrier to F/Ph exchange via pathway 2a is +36.9 kcal/mol, 6–7 kcal/mol higher than those computed along pathways 1a and 1b.

The second metallophosphorane pathway, pathway 2b, is shown in Figure 14 and is based on related work on square-planar Pd systems where transfer of F onto PH_3 was found to be coupled to an isomerization of the metal coordination geometry.⁹⁵ Thus, in this case, as the $\text{P}\cdots\text{F}$ distance is shortened the PH_3 ligand initially trans to PH_2Ph moves with the fluoride to create a vacant site trans to the developing phosphoranide. This led ultimately to the location of a metallophosphorane as an intermediate (**I6**, $E = +30.9$ kcal/mol), formed via $\text{TS}_{\text{cis-1'-16}}$ ($E = +31.3$ kcal/mol). Metallophosphorane **I6** again shows a fairly regular trigonal bipyramidal geometry at phosphorus (angles at P: $\text{C}_{\text{ax}}-\text{P}-\text{Rh} = 100.5^\circ$; $\text{F}_{\text{ax}}-\text{P}-\text{Rh} = 79.9^\circ$; $\text{H}_{\text{eq}}-\text{P}-\text{Rh} = 123^\circ/124^\circ$), and the main difference as compared to $\text{TS}_{\text{cis-1'-15}}$ of pathway 2a is that the phosphoranide moiety is now trans to the vacant site. This results in a shortening of the M– PH_2FPh bond to 2.24 Å, and the fact that **I6** is 6 kcal/mol more stable than $\text{TS}_{\text{cis-1'-15}}$ indicates that PH_2FPh also has a greater trans influence than PH_3 . From **I6** a transition state,

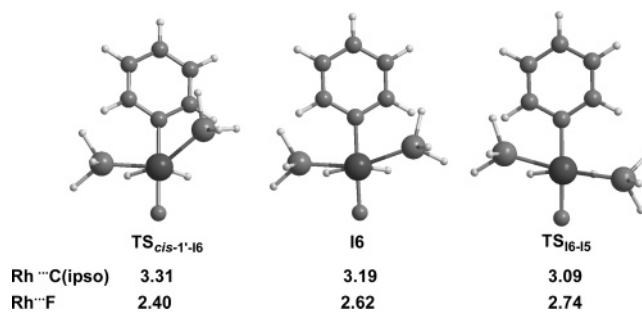


Figure 15. Alternative views of metallophosphorane stationary points along pathway 2b.

TS_{16-15} ($E = +31.0$ kcal/mol), was located that led to the formation of the same η^2 -(P–C) intermediate, **I5**, found along pathway 2a. The potential energy surface around **I6** is therefore extremely flat, with $\text{TS}_{\text{cis-1'-16}}$, **I6**, and TS_{16-15} all being within 0.4 kcal/mol of each other. Despite this, these three stationary points have distinctly different geometries, as seen in the alternative views shown in Figure 15, which emphasize how the increasing $\text{Rh}\cdots\text{F}$ distance is coupled both to a decreasing $\text{Rh}\cdots\text{C}(\text{ipso})$ distance and to the movement of the $\{(\text{PH}_3)_2\text{Rh}\}$ moiety relative to the PH_2FPh ligand. From **I5**, the final delivery of the Ph group to Rh occurs as in pathway 2a via $\text{TS}_{\text{I5-cis-5'}}$.

Overall, the lower energies of the metallophosphorane structures along pathway 2b result in an activation barrier of 31.0 kcal/mol, 6 kcal/mol lower than pathway 2a, but now very similar in magnitude to those computed along pathways 1a/b. The calculations therefore suggest that oxidative addition/reductive elimination (pathways 1a/b) and a metallophosphorane process (pathway 2b) may be competitive as mechanisms for F/Ph exchange in the simple $[(\text{PH}_3)_2(\text{PH}_2\text{Ph})\text{RhF}]$ model system.

To probe the effect of solvent polarity on the energetics of F/Ph exchange, we have recomputed the energies of all stationary points when placed in a continuum with a dielectric

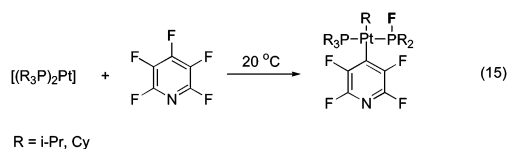
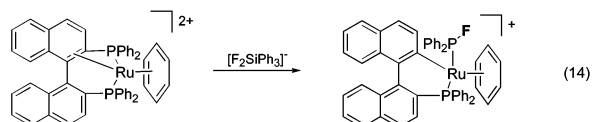
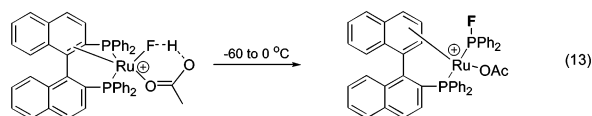
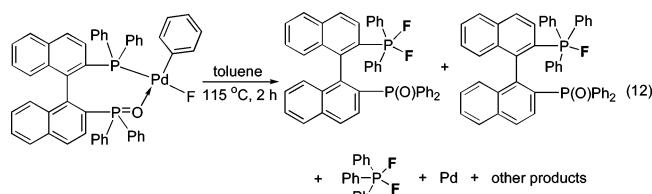
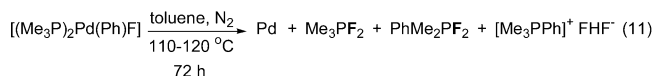
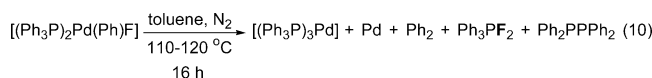
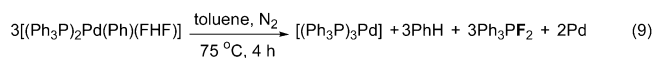
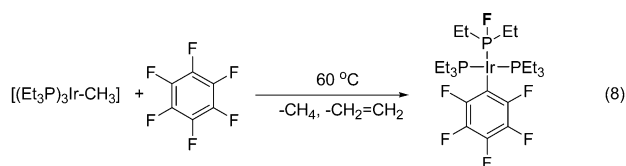
(94) For examples of η^2 -(P–N) and η^2 -(P–O) phosphoranides with group 9 metals, see: (a) Toyota, K.; Yamamoto, Y.; Akiba, K.-Y. *J. Organomet. Chem.* **1990**, 586, 171. (b) De Meester, P.; Lattman, M.; Chu, S. S. C. *Acta Crystallogr., Sect. C* **1987** 43, 162.

(95) Goodman, J.; Macgregor, S. A., unpublished results.

constant equivalent to that of DMSO ($\epsilon = 46.7$). For the direct reaction, **1**' to **5**', the results (in italics in Figures 11–14) indicate that the overall barriers for all four pathways increase in a more polar medium (pathway 1a, +37.2 kcal/mol; pathway 1b, +31.6; pathway 2a, +39.5 kcal/mol; pathway 2b, +34.8 kcal/mol). However, for the reverse reaction, from *cis*-**5**' to *cis*-**1**' (pathways 2a and 2b) and from *cis*-**5**' to *trans*-**1**' (pathway 1b), the computed barriers are all reduced in DMSO, to +31.5, to +26.8, and to +23.3 kcal/mol, respectively. Pathway 1a is the only one of the four that exhibits an increase in the barrier (to +29.2 kcal/mol) for the reaction of **5**' to **1**' in the more polar medium.

Discussion

A half-dozen or so reactions leading to P–C bond cleavage and P–F bond formation at a metal center have been reported in the literature. In 1991, Blum, Frolow, and Milstein⁹⁶ described the first reaction of this type (eq 8). Since then, more examples of P–F bond-forming reactions at Ni,^{37a} Pd^{31–33} (eqs 9–12), Ru⁹⁷ (eqs 13 and 14), and Pt⁹⁸ (eq 15) centers have been published.



In contrast with all of the above examples (eqs 8–15), the F/Ph exchange reaction of [(Ph₃P)₃RhF], **1** (eq 7), is re-

versible. Both the experimental and the theoretical studies indicate that in benzene the interconvertible isomers **1** and **5** are close in energy ($K_{eq} \approx 1$). In other words, $D_{Rh-F} + D_{P-Ph} \approx D_{Rh-Ph} + D_{P-F}$ for the **1/5** pair, in the assumption that entropy change for the Ph/F rearrangement (eq 7) is small.⁹⁹ A P–F bond is usually stronger than a P–C bond. For instance, in PPh₃ and PF₃ the mean P–Ph and P–F bond dissociation enthalpies are ca. 70–80^{100,101} and 115–120^{101,102} kcal/mol, respectively. These values allow us to carefully propose that the Rh–F bond in **1** might be considerably stronger than the Rh–Ph bond in **5** (by ca. 35–50 kcal/mol) and much more thermodynamically stable than a late transition metal–fluorine bond is often thought of. In the absence of experimental values for these bond dissociation enthalpies, support for this statement is gained from the computed homolytic bond dissociation energies of the Rh–F bond in *cis*-**1**' (111.9 kcal/mol) and the Rh–Ph bond of *cis*-**5**' (70.4 kcal/mol).⁹⁹ The calculated value for the difference $D_{Rh-F} - D_{Rh-Ph}$ (41.5 kcal/mol) is within the range of the aforementioned experimental estimation (35–50 kcal/mol).

Various mechanisms have been proposed for reactions 8–15, including radical, oxidative addition, reductive elimination, and metallophosphorane pathways.^{31,96–98} Our calculations on F/Ph exchange in **1** suggest that, in general, two oxidative addition–reductive elimination pathways, 1a (Figure 11) and 1b (Figure 12), and two metallophosphorane pathways, 2a (Figure 13) and 2b (Figure 14), are possible. Two of these four, however, may be disqualified, pathways 1a and 2a. Pathway 2a is less plausible due to its relatively high activation energy barrier of ca. 37 kcal/mol (Figure 13), as compared to ca. 30–31 kcal/mol for the other three (Figures 11, 12, and 14). For pathway 1a, the computed data are inconsistent with the solvent effect data. Experimentally, it was demonstrated that an increase in solvent polarity results in slower rates for the direct reaction (**1** to **5**) and faster rates for the reverse process (**5** to **1**). This is in full accord with the computational data for all the routes, except pathway 1a, where the computational results predict a decrease in the rate of the reaction of **5**' to **1**' upon increasing the polarity of the medium.

For both pathways 1b and 2b remaining under consideration, the experimental and theoretical data for the activation barrier (ca. 23 vs ca. 30 kcal/mol) are in reasonable agreement, even though the simplified *cis*-[(PH₃)₂(PH₂Ph)RhF] model system was used for the calculations, and on this basis both pathways may be feasible. Moreover, there is precedent for key steps in both classes of pathway: aryl transfer to the metal center (Ir) in a metallophosphorane is known,⁸⁹ and reversible oxidative addition of the P–C bond of PPh₃ to [(Et₃P)₄Ni] has also been

(96) Blum, O.; Frolow, F.; Milstein, D. *J. Chem. Soc., Chem. Commun.* **1991**, 258.

(97) (a) den Reijer, C. J.; Woerle, M.; Pregosin, P. S. *Organometallics* **2000**, *19*, 309. (b) den Reijer, C. J.; Dotta, P.; Pregosin, P. S.; Albinati, A. *Can. J. Chem.* **2001**, *79*, 693. (c) Gelbach, T. J.; Pregosin, P. S. *Eur. J. Inorg. Chem.* **2002**, 1907.

(98) Jasim, N. A.; Perutz, R. N.; Whitwood, A. C.; Braun, T.; Izundu, J.; Neumann, B.; Rothfeld, S.; Stammer, H.-G. *Organometallics* **2004**, *23*, 6140.

(99) For $D_{Rh-F} + D_{P-Ph} \approx D_{Rh-Ph} + D_{P-F}$ in the **1/5** pair, it must also be assumed that the Rh–PPh₂Ph bond in **1** is similar in strength to the Rh–PPh₂F bond in **5**. Calculations on our model systems show that the Rh–PH₂Ph bond in *cis*-**1**' is in fact only about 5.3 kcal/mol weaker than the Rh–PH₂F bond in *cis*-**5**'.

(100) Bedford, A. F.; Mortimer, C. T. *J. Chem. Soc.* **1960**, 1622.

(101) Neale, E.; Williams, L. T. D.; Moores, V. T. *J. Chem. Soc.* **1956**, 422.

(102) Brown, T. L.; LeMay, H. E., Jr.; Bursten, B. E. *Chemistry: The Central Science*, 7th ed.; Prentice Hall: Upper Saddle River, NJ, 1997.

demonstrated.¹⁰³ However, on balance, we believe that the metallophosphorane mechanism first reported by one of us⁸⁸ is more plausible, for the following reasons:¹⁰⁴

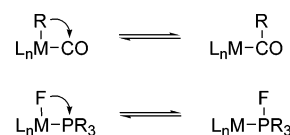
(1) Oxidative addition to low-valent transition metals such as Rh(I) and Pd(0) usually requires a vacant coordination site and hence is commonly decelerated by extra phosphine.¹⁰⁵ This is also true for P–C oxidative addition reactions of PPh_3 to mononuclear Ni(0),¹⁰³ Pd(0),¹⁰³ and Rh(I),¹⁰⁶ which are all inhibited by extra phosphine. In contrast, reactions 2, 3, and 7 are not influenced by even a large excess of PPh_3 . Moreover, phosphine deficiency slows down the F/Ph exchange, as it leads to the dimer $[(\text{Ph}_3\text{P})_4\text{Rh}_2(\mu\text{-F})_2]$ that is highly thermally stable (see above). In this species, the movement of the bridging F is restricted and the ability of F to act as an internal nucleophile may be lost or at least diminished. This is further circumstantial evidence for pathway 2b over 1b, as $[(\text{Ph}_3\text{P})_4\text{Rh}_2(\mu\text{-F})_2]$ still should be able to undergo P–C bond cleavage even if the subsequent P–F bond formation were not possible.

(2) Oxidative addition of the P–C bond of a tertiary phosphine to a metal center most frequently leads to di- and polynuclear complexes with PR_2 bridges.^{103,106,107} Such species have never been observed in our studies of the reactions of **1** or **5**.

(3) Attempted preparation of $[(\text{Ph}_3\text{P})_3\text{IrF}]$ was carried out from $[(\text{COD})_2\text{Ir}_2(\mu\text{-OH})_2]$, 12 equiv of PPh_3 , and TREAT HF, or from $[(\text{Ph}_3\text{P})_3\text{IrCl}]$ and AgF under sonication in benzene. Both reactions resulted in complex mixtures containing PPh_3 -cyclo-metalated species (upfield multiplet resonances around -40 to -70 ppm in the ^{31}P NMR)¹⁰⁸ but no P–F bond containing products. Hence, we conclude that while the Ir complexes are apparently more prone to oxidative addition (in this case cyclometalation) than **1**, P–F bond formation at the Ir center does not occur.

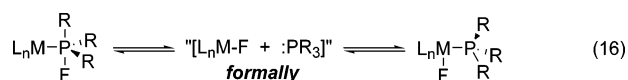
In simplified terms, the first step in the new metallophosphorane mechanism^{88,95} may be regarded as somewhat similar to migratory insertion involving transfer of a metal alkyl ligand onto CO¹⁰⁹ (Scheme 4). Thus, F acts as an internal nucleophile attacking phosphine, and the reduction in nucleophilic character

Scheme 4



arising from H-bonding to MeCN or DMSO may contribute to the reduced reactivity of **1** observed in these solvents.

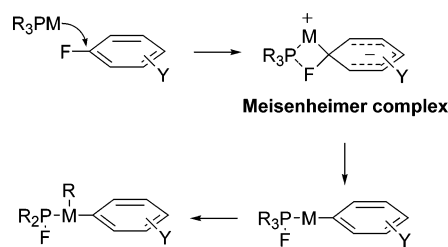
Alternatively, the F/Ph rearrangement (eq 7) via a metallophosphorane might be formally viewed as an intramolecular version of the concerted fragmentation process $\text{PR}_5 \rightleftharpoons \text{PR}_3 + \text{R}_2$,¹¹⁰ in which the R_2 product contains a Lewis acid center and hence appears coordinated to the PR_3 formed in the same reaction (eq 16).



The thermal decomposition of aryl palladium fluorides (eqs 10–12) leading to P–F bond formation might also proceed via a metallophosphorane. Two independent, competing reaction paths have been observed for the decomposition of $[(\text{Ph}_3\text{P})_2\text{-Pd}(\text{C}_6\text{D}_5)\text{F}]$.³¹ One of the two involves reversible P–C reductive elimination to give a phosphonium cation, a process that is inhibited by extra phosphine.^{31,111} The other decomposition path leads to P–F bond formation and is not influenced by extra phosphine,³¹ much like the F/Ph rearrangement reaction of **1**. In addition, methyl/phenyl exchange has also been observed in $[(\text{Ph}_3\text{P})_2\text{Pd}(\text{I})\text{Me}]$ ¹¹² and has been shown not to be inhibited by free phosphine, and so we suggest that it too may be mediated by a metallophosphorane. We also propose that in certain cases, P–F bond formation via a metallophosphorane might not involve a metal fluoride intermediate. For instance, oxidative addition of the reactive C–F bond of hexafluorobenzene and pentafluoropyridine to some tertiary phosphine metal complexes may occur via an $\text{S}_{\text{N}}\text{Ar}$ -type mechanism with extra stabilization of the Meisenheimer intermediate by P–F coordination. The latter also makes the basic and highly reactive fluoride a better leaving group (Scheme 5). Such a mechanism might be operative in reactions similar to those shown in eqs 8 and 15.

Perutz, Braun, and co-workers⁹⁸ recently reported that while oxidative addition of pentafluoropyridine to $[(\text{R}_3\text{P})_2\text{Pd}]$ ($\text{R} = i\text{-Pr}$ or Cy) produced $[(\text{R}_3\text{P})_2\text{Pd}(\text{C}_5\text{F}_4\text{N})\text{F}]$, the reaction of the same substrate with similar platinum complexes $[(\text{R}_3\text{P})_2\text{Pt}]$ ($\text{R} = i\text{-Pr}$ or Cy) led to P–F and Pt–R bond formation (eq 15).

Scheme 5



(103) Fahey, D. R.; Mahan, J. E. *J. Am. Chem. Soc.* **1976**, *98*, 4499.

(104) A reviewer proposed that the F/Ph rearrangement might be catalyzed by an adventitious source of proton or hydrogen bond donor, which could coordinate to the F ligand thus weakening the Rh–F bond. In our experiments, special precautions were taken to avoid the presence of acid and water. Our kinetic results were consistently reproducible for both the direct and the reverse reactions, suggesting that a significant contribution from catalysis by acid or water was unlikely. Following the reviewer's recommendation, we ran the reactions of **1** going to **5** and of **5** going to **1** under our standard anhydrous conditions (see the Experimental Section) in the presence and in the absence of dry CsF as a base. For these experiments, CsF was calcined under vacuum, brought in the glovebox, ground up to a fine powder, vacuum-calcined again, and stored in the glovebox. The reaction of **1** in a Teflon liner at 70 °C was not influenced by CsF (30 equiv per Rh), reaching equilibrium after 1 h (^{19}F NMR), much like the similar reaction previously conducted in the absence of CsF in glass (see Figure 5A of the Supporting Information). Neither CsF (20 equiv) nor $p\text{-C}_6\text{H}_4\text{SO}_3\text{H}\cdot\text{H}_2\text{O}$ (1 mol % to [Rh]) affected significantly the reaction of **1** at 60 °C. No substantial effect of CsF (22 equiv) was observed on conversion of **5** to **1** at the same temperature (60 °C) after 20, 50, and 90 min. We conclude therefore that, under our conditions, acid catalysis is unlikely to be the main channel for the F/Ph rearrangement.

(105) (a) For instance, $[(\text{Ph}_3\text{P})_2\text{RhCl}]$ is at least 2 orders of magnitude more reactive toward oxidative addition of H_2 than $[(\text{Ph}_3\text{P})_3\text{RhCl}]$: Halpern, J.; Wong, C. S. *J. Chem. Soc., Chem. Commun.* **1973**, 629. (b) In the oxidative addition of aromatic iodides to $[(\text{Ph}_3\text{P})_n\text{Pd}]$ ($n = 3, 4$), the reactive Pd(0) species is $[(\text{Ph}_3\text{P})_2\text{Pd}]$: Fauvarque, J.-F.; Pflüger, F.; Troupel, M. *J. Organomet. Chem.* **1981**, *208*, 419.

(106) Lewin, M.; Aizenshtat, Z.; Blum, J. *J. Organomet. Chem.* **1980**, *184*, 255.

(107) Garrou, P. E. *Chem. Rev.* **1985**, *85*, 171.

(108) Dahlenburg, L. *J. Organomet. Chem.* **1983**, *251*, 347. Bennett, M. A.; Bhargava, S. K.; Ke, M.; Willis, A. C. *Dalton Trans.* **2000**, 3537.

(109) For a review, see: Cavell, K. J. *Coord. Chem. Rev.* **1996**, *155*, 209.

(110) Hoffmann, R.; Howell, J. M.; Muetterties, E. L. *J. Am. Chem. Soc.* **1972**, *94*, 3047.

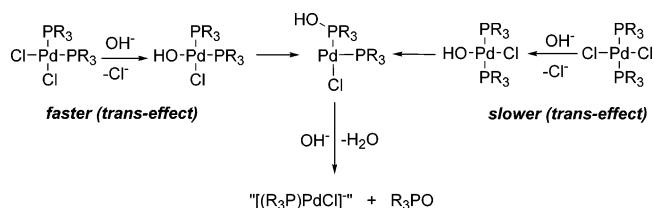
(111) (a) Kong, K.-C.; Cheng, C.-H. *J. Am. Chem. Soc.* **1991**, *113*, 6313. (b) Goodson, F. E.; Wallow, T. I.; Novak, B. M. *J. Am. Chem. Soc.* **1997**, *119*, 12441.

(112) Morita, D. K.; Stille, J. K.; Norton, J. R. *J. Am. Chem. Soc.* **1995**, *117*, 8576.

Attempts to detect a Pt–F intermediate failed as even at lower temperatures only P–F bond formation was observed. We found that [(Cy₃P)₂Pt] reacted with C₆F₆ in THF at 65 °C ca. 5 times faster than [(Cy₃P)₂Pd], the reaction products being [(Cy₃P)Pt-(Cy₂PF)(Cy)(C₆F₅)] and [(Cy₃P)₂Pd(C₆F₅)(F)], respectively (see the Experimental Section), in full accord with the Perutz–Braun⁹⁸ data on similar reactions with C₅F₅N. In contrast, reactions of [(Cy₃P)₂M] (M = Pd, Pt) with neat chlorobenzene at 25 °C furnished [(Cy₃P)₂M(Ph)(Cl)] regardless of the nature of the metal, the reaction of [(Cy₃P)₂Pd] being slightly faster (k_{Pd}/k_{Pt} = ca. 1.2; see the Experimental Section). The different reaction outcomes and the fact that k_{Pd}/k_{Pt} < 1 for the reaction with C₆F₆ but k_{Pd}/k_{Pt} > 1 for the reaction with PhCl indicate that different mechanisms might be involved. While the reaction of C₅F₅N or C₆F₆ with [(Cy₃P)₂Pd] might occur via a three-center mechanism, the more nucleophilic Pt complex might react via an S_NAr-type path, as shown in Scheme 5. Likewise, an elegant study by Fóa and Cassar clearly demonstrated that oxidative addition of the C–Cl bond of *p*-XC₆H₄Cl to [(Ph₃P)₃Ni] can occur via two distinctive mechanisms, probably S_NAr for strongly electron-withdrawing X and 3-center for all other substituents.¹¹³

Like fluoride,⁸⁷ some hard O-anions¹¹⁴ such as acetate¹¹⁵ or hydroxide^{116,117} have been reported to promote the clean and often remarkably facile reduction of Pd(II), Pt(II), Rh(III), and some other metals at the expense of a tertiary phosphine ligand in the inner sphere. With OH[−] (Scheme 6), the reaction is initiated via M–OH bond formation and subsequently proceeds with retention of configuration at P.¹¹⁷ These observations are consistent with an intramolecular attack of OH[−] on phosphine and thus may well involve the intermediacy of a metallophosphorane.^{88,95}

Scheme 6



In contrast to its fluoro analogue, Wilkinson's catalyst does not undergo transformations such as those shown in eqs 2 and 3. Preliminary calculations¹¹⁶ on *cis*-[(PH₃)₂(PH₂Ph)RhCl], the chloro congener of *cis*-**1'**, have established that Cl/Ph exchange via pathway 1a has a barrier of ca. 41 kcal/mol. To date, we have not succeeded in locating metallophosphorane structures analogous to **TS**_{*cis*-1'-15} (Figure 13) or **I6** (Figure 14) that were located along pathways 2a and 2b in the fluoro system. All attempts to optimize such structures resulted in elongation of the P–Cl distance, often with Cl transfer back to Rh. Mapping of the potential energy surfaces around these putative metallophosphorane structures was performed by systematically varying

the Rh···Cl and Rh···C(ipso) distances, and these calculations indicated that any metallophosphorane species would be at least 40 kcal/mol higher in energy than *cis*-[(PH₃)₂(PH₂Ph)RhCl]. Thus, the barriers for Cl/Ph exchange are at least 10 kcal/mol higher than those for F/Ph exchange, and these higher barriers in the case of the chloro species are consistent with the nonobservation of processes based on Cl/Ph exchange in Wilkinson's catalyst under comparable conditions (80–100 °C). It has indeed been reported¹⁰⁶ that the thermal decomposition of Wilkinson's catalyst to Ph₂ (and presumably Rh–PPh₂) species requires hours at 140–180 °C to occur to observable conversions.

Conclusions

The fluoride congener of Wilkinson's catalyst, [(Ph₃P)₃RhF] (**1**), has been synthesized, fully characterized, and found to exhibit distinctive reactivity. In sharp contrast with Wilkinson's catalyst, **1** easily cleaves the inert C–Cl bond of nonactivated chloroarenes (chlorobenzene, *p*-chlorotoluene) under mild conditions to produce *trans*-[(Ph₃)₂Rh(Ph₂PF)(Cl)] as a result of C–Cl, Rh–F, and P–C bond cleavage and C–C, Rh–Cl, and P–F bond formation. The thermal decomposition of **1** in benzene (2–3 h at 80 °C) leads to a 1:1 mixture of *trans*-[(Ph₃)₂Rh(Ph₂PF)(F)] and [(Ph₃)₃RhPh], which easily undergoes cyclometalation to [(Ph₃)₂Rh(Ph₂PC₆H₄)].

The chloroarene activation and thermal decomposition reactions of **1** have a common first step involving the facile and reversible F/Ph rearrangement reaction of **1** to *cis*-[(Ph₃)₂Rh(Ph)(Ph₂PF)] (**5**). The latter has been isolated and fully characterized in solution and in the solid state (X-ray). Kinetic studies of the interconversion of **1** and **5** indicated a unimolecular process that is not influenced by extra phosphine, with $\Delta H^\ddagger = 22.0 \pm 1.2$ kcal mol^{−1} and $\Delta S^\ddagger = -10.0 \pm 3.7$ eu, and the corresponding Arrhenius parameters $E_a = 22.7 \pm 1.2$ kcal mol^{−1} and $\log(A/s^{-1}) = 11.1 \pm 0.8$. Density functional calculations on a [(PH₃)₂(PH₂Ph)RhF] model system identified two possibly competing mechanisms: (i) P–C oxidative addition with subsequent F–P reductive elimination (pathway 1b) and (ii) F transfer to produce a metallophosphorane,^{88,95} followed by Ph transfer to Rh (pathway 2b). Although both pathways display similar activation barriers for the simple [(PH₃)₂(PH₂Ph)RhF] model system, a number of experimental observations suggest that the metallophosphorane mechanism is more plausible. Analysis of some literature data likewise strengthens the notion that certain reactions resulting in P–F, P–O, and P–C bond formation at a metal center might also be mediated by metallophosphorane species.^{88,95}

Experimental Section

All chemicals were purchased from Aldrich and Strem chemical companies and used as received. Complexes [(COD)₂Rh₂(μ-OH)₂],⁶¹ [(Ph₃P)₄Rh₂(μ-OH)₂],⁶³ [(Ph₃P)₃RhPh],⁵⁸ [(Cy₃P)₂Pd],¹¹⁸ [(Cy₃P)₂Pt],¹¹⁹ [(COD)₂Pt],¹²⁰ [(COD)₂Ir₂(μ-OH)₂],¹²¹ and [(Ph₃P)₃IrCl]¹²² were prepared as described in the literature. The solvents were thoroughly dried using standard techniques and stored over freshly calcined molecular sieves (4 Å) in a glovebox. All manipulations with the Rh fluoride

(113) Fóa, M.; Cassar, L. *J. Chem. Soc., Dalton Trans.* **1975**, 2572.

(114) For a recent overview of such reactions, see section 2.2 in: Grushin, V. *Chem. Rev.* **2004**, *104*, 1629.

(115) For accounts of the detailed studies of the catalytically important reaction of Pd(OAc)₂ with R₃P leading to Pd(0) and R₃PO, see: Amatore, C.; Jutand, A. *Acc. Chem. Res.* **2000**, *33*, 314; *J. Organomet. Chem.* **1999**, *576*, 254.

(116) Gonzalez-Carrera, V.; Goodman, J.; Macgregor, S. A., unpublished results.

(117) Grushin, V. V.; Alper, H. *Organometallics* **1993**, *12*, 1890.

(118) Grushin, V. V.; Bensimon, C.; Alper, H. *Inorg. Chem.* **1994**, *33*, 4804.

(119) Fomies, J.; Green, M.; Spencer, J. L.; Stone, F. G. A. *J. Chem. Soc., Dalton Trans.* **1977**, 1006.

(120) Walther, D.; Heubach, K.; Böttcher, L.; Schreer, H.; Görls, H. *Z. Anorg. Allg. Chem.* **2002**, *628*, 20.

(121) Green, L. M.; Meek, D. W. *Organometallics* **1989**, *8*, 659.

(122) Bennett, M. A.; Latten, J. L. *Inorg. Synth.* **1989**, *26*, 200.

complexes and products of their transformations were carried out under nitrogen in a glovebox. NMR spectra were obtained with Bruker Avance DRX400 and Varian Unity Inova systems, both operating at 400 MHz. NMR spectral simulations were performed using Nuts Professional processing software (Acorn NMR, Livermore, CA). The kinetic NMR data in Figure 9 and in the Supporting Information were analyzed as described in the text using the lsqnonlin function from the MATLAB Optimization Toolbox (MATLAB Version 7, The Mathworks, Inc., Natick, MA). A Bruker-CCD instrument was used for single-crystal X-ray diffraction studies. Microanalyses were performed by Micro-Analysis, Inc., Wilmington, DE, and Galbraith Laboratories, Inc., Knoxville, TN.

Synthesis of [(Ph₃P)₃RhF] (1). (a) To a stirring mixture of [(COD)₂Rh₂(μ-OH)₂] (0.15 g; 0.33 mmol), PPh₃ (1.15 g; 4.25 mmol), and ether (8 mL) was added Et₃N·3HF (TREAT HF; 37 μL; 0.23 mmol). After the mixture was vigorously stirred for 2 h, the orange-yellow microcrystalline precipitate was separated by filtration, thoroughly washed with ether, and dried under vacuum. The yield of **1** was 0.56 g (94%). Anal. Calcd for C₅₄H₄₅FP₃Rh, %: C, 71.4; H, 5.0. Found, %: C, 71.2; H, 5.3. ¹H NMR (C₆D₆, 20 °C), δ: 7.0 (m, 3H, *m,p*-Ph); 7.9 (m, 2H, *o*-Ph). For the ¹⁹F and ³¹P data, see Table 2. (b) TREAT HF (90 μL; 0.56 mmol) was added to a vigorously stirring mixture of [(COD)₂Rh₂(μ-OH)₂] (0.34 g; 0.75 mmol), PPh₃ (2.5 g; 9.5 mmol), and ether (15 mL). After being stirred for 3 h at room temperature, the orange-yellow precipitate was separated, washed with ether, and dried under vacuum. The yield of **1** was 1.22 g (90%). X-ray quality crystals were obtained by quickly dissolving the complex in warm benzene at vigorous stirring, adding hexanes to the warm, solid-free orange solution, and leaving the mixture at room temperature overnight. (c) This experiment exemplifies the synthesis of **1** using substoichiometric quantities of TREAT HF to avoid contamination with bifluoride, for kinetic studies. To a stirring mixture of [(COD)₂Rh₂(μ-OH)₂] (0.160 g; 0.35 mmol), PPh₃ (1.25 g; 4.77 mmol), and ether (12 mL) was added Et₃N·3HF (TREAT HF; 35 μL; 0.22 mmol). After the mixture was vigorously stirred for 2 h, the orange-yellow microcrystalline precipitate was separated by filtration, thoroughly washed with THF, benzene, and ether, and dried under vacuum overnight. The yield of **1** was 0.38 g (65%, as calculated on the HF source).

Synthesis of [(Ph₃P)₄Rh₂(μ-F)₂]. Solid [(Ph₃P)₄Rh₂(μ-OH)₂] (0.22 g; 0.17 mmol) was dissolved in hot benzene (12 mL), the heater was removed, and the orange solution was treated, at vigorous stirring, with Et₃N·3HF (TREAT HF; 20 μL; 0.12 mmol). The color turned reddish-orange immediately. After 15 min of vigorous stirring, the solution was filtered through cotton wool, reduced in volume to ca. 4 mL, and treated with hexanes (8 mL). After 1 h, the red-orange crystals were separated, washed with hexanes (3 × 6 mL), and dried under vacuum. The yield of [(Ph₃P)₄Rh₂(μ-F)₂] was 0.155 g. The mother liquor and the washings were combined to produce additional quantities of [(Ph₃P)₄Rh₂(μ-F)₂] (0.04 g) upon standing at room temperature for 2 days. Overall yield: 0.195 g (88%). This very air-sensitive compound is insoluble in ether, alkanes, and cycloalkanes, poorly soluble in benzene and THF, and is decomposed instantly by dichloromethane. Anal. Calcd for C₇₂H₆₀F₂P₄Rh₂, %: C, 66.9; H, 4.7. Found, %: C, 66.2; H, 4.7. ¹H NMR (C₆D₆, 20 °C), δ: 6.8 (m, 3H, *m,p*-Ph), 7.8 (m, 2H, *o*-Ph). ¹⁹F NMR (C₆D₆, 20 °C), δ: -323.7 (m; *J*_{Rh-F} = ca. 40 Hz). ³¹P NMR (C₆D₆, 20 °C), δ: 60.5 (m; *J*_{Rh-P} = 207.7 Hz; *J*_{P-F} = 195.5 Hz). The ¹⁹F and ³¹P NMR spectral patterns are complex and similar to those previously reported⁴¹ for the *i*-Pr₃P analogue, [(*i*-Pr₃P)₄Rh₂(μ-F)₂], an AA'A''A'''MM'XX' spin system. For details, see ref 53.

Reaction of 1 with PhCl or TolCl. (a) A mixture of **1** (0.215 g; 0.24 mmol) and chlorobenzene (1 mL) was stirred at 100 °C (oil bath) for 2.5 h. The mixture was cooled to room temperature, treated with toluene (3 mL) and hexanes (3 mL), and left overnight. The crystalline solid was separated and quickly extracted with toluene (8 mL) at reflux. The orange extract was filtered hot and treated with hexanes (4 mL).

After 4 h at room temperature, yellow crystals of **2** were separated and dried under vacuum. The yield of spectroscopically pure **2** was 0.103 g (50%). The product was recrystallized from dichloromethane–hexanes before combustion analysis. Anal. Calcd for C₄₈H₄₀ClFP₃Rh, %: C, 66.5; H, 4.7. Found, %: C, 65.6; H, 4.8. For the NMR characterization, see Table 2. (b) **1** (63 mg) was reacted with PhCl (0.3 mL) as described above. The reaction mixture was diluted with pentane (4 mL), filtered through silica gel, and analyzed by GC–MS to reveal the formation of biphenyl. (c) **1** (83 mg) was reacted with *p*-chlorotoluene, as described above. The reaction mixture was diluted with pentane (4 mL) and filtered through silica gel. GC–MS analysis of the colorless filtrate indicated the formation of 4-methylbiphenyl and biphenyl in a 1000:8 ratio.

Thermal Decomposition of 1. A 5-mm NMR tube was charged with **1** (40 mg) and benzene (0.5 mL), sealed, and heated (with occasional swirling until **1** had all dissolved) at 80 °C (oil bath). Reaction progress was monitored by ³¹P and ¹⁹F NMR. After 3 h at 80 °C (ca. 90% conversion), the mixture contained two complexes, **3** and **4** in a 1:1 molar ratio, as indicated by the NMR data (see Table 2 and ref 66).

Thermal Decomposition of [(Ph₃P)₃RhPh]. A solution of [(Ph₃P)₃RhPh] (ca. 30 mg) in benzene (0.6 mL) was heated at 80 °C (oil bath) for 1 h. ³¹P NMR analysis of the orange reaction solution revealed the formation of **4** via cyclometalation in ca. 100% selectivity.

Reaction of [(Ph₃P)₃RhPh] with PhCl. A 5-mm NMR tube was charged with [(Ph₃P)₃RhPh] (ca. 30 mg) and chlorobenzene (0.6 mL), sealed, and heated at 80 °C (oil bath) for 1 h. ³¹P NMR analysis of the orange reaction solution revealed the formation of [(Ph₃P)₃RhCl].

Preparation of cis-[(Ph₃P)₂Rh(Ph)(Ph₂PF)] (5). A mixture of **1** (0.39 g; 0.43 mmol), PPh₃ (0.74 g; 2.82 mmol), and benzene (18 mL) in a closed vessel was stirred at 75 °C (oil bath) for 1 h. The mixture was worked up in a glovebox. The solution was evaporated to leave a dark red-brown residue, which was treated with ether (10 mL). After the mixture was stirred for 10 min, the orange precipitate was filtered off. The filtrate was reduced in volume to ca. 5 mL and treated with hexanes (5 mL). Yellow crystals of **5** began to form. After 30 min, more hexanes (2 mL) were added. After 2 h, the yellow crystals of **5** were separated, washed with ether (3 × 2 mL), hexanes (2 × 2 mL), and dried. Keeping the combined mother liquor and the washings at -20 °C overnight produced an extra quantity of **5** as yellow needles. Both crops of **5** were combined, dissolved in benzene (3 mL), and the solution was evaporated with a nitrogen flow to ca. 1 mL. Hexanes (1 mL) were added, followed by more hexanes (9 mL) after 10 min. After the mixture was kept at -20 °C for 2 weeks, yellow crystals of spectroscopically pure **5** were separated, washed with hexanes, and dried under vacuum. The yield of **5** was 0.115 g (29%). X-ray quality crystals of **5**·2C₆H₆ and **5**·Et₂O were obtained by recrystallization from benzene and benzene–ether–hexanes, respectively. Anal. Calcd for C₅₈H₅₅FOP₃Rh (**5**·Et₂O), %: C, 70.9; H, 5.6. Found, %: C, 70.1; H, 5.5. ¹H NMR (C₆D₆, 20 °C), δ: 6.6–6.8 (m, 3H, *m,p*-PhRh), 7.9 (m, 42H, PhP and *o*-PhRh). For the ¹⁹F and ³¹P NMR spectra, see Figures 7 and 8.

Reactions of [(Cy₃P)₂M] (M = Pd, Pt) with PhCl. Both complexes used for these experiments were >99% pure and extra phosphine-free (³¹P NMR). Two samples were prepared: [(Cy₃P)₂Pd] (17 mg; 0.026 mmol) in PhCl (0.55 mL) and [(Cy₃P)₂Pt] (20 mg; 0.026 mmol) in PhCl (0.55 mL). The reactions were monitored via ³¹P NMR. After 20, 90, and 115 h at room temperature, the conversions of the Pd and Pt complexes to [(Cy₃P)₂M(Ph)Cl] were 25% and 20%, 69% and 55%, and 84% and 69%, respectively. From these data, the value of *k*_{Pd}/*k*_{Pt} was calculated at ca. 1.2. The chemical shifts and *J*_{P-Pt} values observed for [(Cy₃P)₂Pd],¹¹⁸ [(Cy₃P)₂Pt],¹¹⁹ [(Cy₃P)₂Pd(Ph)Cl],^{55c} and [(Cy₃P)₂Pt(Ph)Cl]¹¹⁹ were similar to those reported in the literature. Oxidative addition reactions of chlorobenzene to [(Cy₃P)₂Pd(dba)],^{55c} and to [(Cy₃P)₂Pt],¹¹⁹ have been reported previously.

Table 5. A Summary of Crystallographic Data for **3**, **5**·2C₆H₆, **5**·Et₂O, and **6**

	3	5 ·2C ₆ H ₆	5 ·Et ₂ O	6
empirical formula	C ₄₈ H ₄₀ F ₂ P ₃ Rh	C ₆₆ H ₅₇ FP ₃ Rh	C ₅₈ H ₅₅ FOP ₃ Rh	C ₄₈ H ₄₁ F ₃ P ₃ Rh
FW	850.62	1064.94	982.84	870.63
cryst color, form	gold, irreg. block	gold, irreg. block	clear, needle	gold, irreg. block
cryst system	monoclinic	monoclinic	orthorhombic	monoclinic
space group	<i>P</i> 2(1)/ <i>c</i>	<i>P</i> 2(1)/ <i>n</i>	<i>P</i> 2(1)2(1)2(1)	<i>P</i> 2(1)/ <i>n</i>
<i>a</i> (Å)	12.865(4)	13.3165(7)	9.702(6)	12.4782(9)
<i>b</i> (Å)	10.424(3)	19.8008(11)	22.373(13)	20.1446(14)
<i>c</i> (Å)	29.519(8)	20.2300(11)	22.947(13)	16.0477(11)
α (deg)	90	90	90	90
β (deg)	99.343(5)	100.2060(10)	90	95.7850(10)
γ (deg)	90	90	90	90
<i>V</i> (Å ³)	3906.1(19)	5249.8(5)	4981(5)	4013.3(5)
<i>Z</i>	4	4	4	4
density (g/cm ³)	1.446	1.347	1.311	1.441
abs. μ (mm ⁻¹)	0.604	0.462	0.482	0.593
<i>F</i> (000)	1744	2208	2040	1784
cryst size (mm)	0.34 × 0.13 × 0.08	0.30 × 0.30 × 0.28	0.22 × 0.01 × 0.01	0.46 × 0.46 × 0.15
temp (°C)	−100	−100	−100	−100
scan mode	<i>ω</i>	<i>ω</i>	<i>ω</i>	<i>ω</i>
detector	Bruker-CCD	Bruker-CCD	Bruker-CCD	Bruker-CCD
θ _{max} (deg)	29.19	28.71	22.39	28.3
no. obsd. refs	73 287	43 223	30 183	33 129
no. uniq. refs	10 507	13 307	6393	9955
<i>R</i> _{merge}	0.0598	0.0393	0.1707	0.0286
no. params	487	641	577	501
<i>R</i> indices [<i>I</i> > 2σ(<i>I</i>)] ^a	w <i>R</i> ₂ = 0.089, <i>R</i> ₁ = 0.037	w <i>R</i> ₂ = 0.0844, <i>R</i> ₁ = 0.0331	w <i>R</i> ₂ = 0.096, <i>R</i> ₁ = 0.052	w <i>R</i> ₂ = 0.075, <i>R</i> ₁ = 0.030
<i>R</i> indices (all data) ^a	w <i>R</i> ₂ = 0.094, <i>R</i> ₁ = 0.062	w <i>R</i> ₂ = 0.092, <i>R</i> ₁ = 0.045	w <i>R</i> ₂ = 0.107, <i>R</i> ₁ = 0.093	w <i>R</i> ₂ = 0.078, <i>R</i> ₁ = 0.042
<i>S</i> ^b	0.973	1.039	0.87	1.08
max diff peak, hole (e/Å ³)	0.85, −0.67	0.43, −0.48	0.58, −0.57	0.58, −0.28

^a $R_1 = \sum ||F_o| - |F_c|| / \sum |F_o|$, $wR_2 = \{ \sum [w(F_o^2 - F_c^2)^2] / \sum [w(F_o^2)] \}^{1/2}$ (sometimes denoted as R_w2). ^b $GOF = S = \{ \sum [w(F_o^2 - F_c^2)^2] / (n - p) \}^{1/2}$, where n is the number of reflections, and p is the total number of refined parameters.

Reactions of [(Cy₃P)₂M] (M = Pd, Pt) with C₆F₆. Both complexes used for these experiments were >99% pure and extra phosphine-free (³¹P NMR). Two samples were prepared: [(Cy₃P)₂Pd] (48 mg; 0.07 mmol) and C₆F₆ (10 μL) in THF (0.65 mL) and [(Cy₃P)₂Pt] (55 mg; 0.07 mmol) and C₆F₆ (10 μL) in THF (0.65 mL). The reactions were run in sealed 5-mm NMR tubes at 70 °C (oil bath) and monitored by ³¹P and ¹⁹F NMR. After 24 h, the conversions of the Pd and Pt complexes to *trans*-[(Cy₃P)₂Pd(C₆F₅)F] and [(Cy₃P)Pt(Cy₂PF)(Cy)(C₆F₅)] were 3% and 15%, correspondingly. NMR data for *trans*-[(Cy₃P)₂Pd(C₆F₅)F], δ: ¹⁹F: −110.1 (m, 2F, C₆F₅), −164.8 (m, 1F, C₆F₅), −165.8 (m, 2F, C₆F₅), −325.0 (br s, 1F, Pd−F). ³¹P: 31.6 (d, *J*_{P−F} = 16 Hz). NMR data for [(Cy₃P)Pt(Cy₂PF)(Cy)(C₆F₅)], δ: ¹⁹F: −111.2 (m, 2F, *J*_{F−Pt} = 196 Hz, *o*-C₆F₅), −164.2 (m, 2F, C₆F₅), −164.4 (m, 1F, C₆F₅), −175.8 (ddt, 1F, *J*_{F−P} = 904.6 and 37.5 Hz, *J*_{F−Pt} = 375 Hz, P−F). ³¹P: 19.2 (dd, 1P, *J*_{P−F} = 37.5 Hz, *J*_{P−P} = 443.7 Hz, *J*_{P−Pt} = 2722 Hz, Cy₃P), 181.7 (dd, 1P, *J*_{P−F} = 904.6 Hz, *J*_{P−P} = 443.7 Hz, *J*_{P−Pt} = 3851 Hz, Cy₂PF). These NMR characteristics are similar to those reported⁹⁸ for *trans*-[(Cy₃P)₂Pd(4-C₅F₄N)F] and [(Cy₃P)Pt(Cy₂PF)(Cy)(4-C₅F₄N)].

Kinetic Measurements. Samples of **1** and **5** for kinetic studies were prepared by the methods described above. Because **1** cannot be purified by recrystallization, any excess of TREAT HF was strictly avoided in its synthesis to prevent contamination with bifluoride. Precautions were taken to avoid the presence of adventitious water in the samples. Only brand new, previously unused Wilmad 528-PP NMR tubes were employed, which were carefully vacuum oven-dried prior to sample preparation.^{104,123}

One-dimensional ³¹P, ¹⁹F NMR and kinetic data were acquired on a Varian Unity Inova system operating at 400 MHz. For the kinetic data obtained by ¹⁹F NMR, the transmitter was placed at −180 ppm,

approximately centered between the Rh−F region (−260 to −285 ppm) and the P−F region (−110 to −130 ppm). A spectral width of 100 kHz was used to observe additional decomposition products. An acquisition time of 0.5 s was used in conjunction with a recycle delay of 1 s and a pulse width of 55°. Temperature calibration using an ethylene glycol standard indicated insignificant deviations (<±0.2 °C) from the thermocouple set point in the range used for the kinetic data. Full details of the kinetic studies are presented in the Supporting Information.

Solvent Effect Studies. (a) In a drybox, a stock solution was prepared of **1** (18 mg), PPh₃ (146 mg), and dry, O₂-free benzene (4 mL). Three 5-mm NMR tubes were charged with 0.7 mL of this freshly prepared solution. To these three tubes, rigorously anhydrous benzene (0.2 mL; control sample **A**), acetonitrile (0.2 mL; sample **B**), and DMSO (0.2 mL; sample **C**) were added. The tubes were swirled to ensure homogeneity, sealed, and brought out. The samples were analyzed by ¹⁹F NMR after 17 h at 25 °C, to determine the conversion to **5** at 19%, <5%, and <5% for **A**, **B**, and **C**, respectively. All three samples were then placed in an oil bath at 40 °C for 2 h, and analyzed again. The conversion to **5** was calculated at 19%, <5%, and <5% for **A**, **B**, and **C**, respectively. Analysis by ³¹P NMR indicated that partial decomposition of **1** had taken place in samples **B** (<20% to [(Ph₃P)₃Rh(MeCN)]⁺) and **C** (<30–40% to unidentified products). ³¹P NMR characteristics for the [(Ph₃P)₃Rh(MeCN)]⁺ were in accord with the literature data:¹²⁴ 33.5 ppm, 2P, dd, *J*_{P−P} = 39.4 Hz, *J*_{P−Rh} = 139.8 Hz; 45.8 ppm, 1P, dt, *J*_{P−Rh} = 172.7 Hz. (b) Three samples were prepared as described above, except **5** was used instead of **1**. The samples were analyzed by ¹⁹F NMR after 1 h at 40 °C, to determine the conversion to **3** at <5%, 60%, and 60% for **A**, **B**, and **C**, respectively. Analysis of **B** by ³¹P NMR indicated the formation of stoichiometric amounts of [(Ph₃P)₃−Rh(Ph)], due to the facilitated ligand exchange between **1** produced and the as yet unreacted **5** (see Schemes 1 and 2), and trace quantities

(123) Our initial kinetic studies were carried out with samples placed in both 5-mm and 10-mm NMR tubes, with and without inert Teflon liners. These variations in the nature of the surface (glass vs Teflon) and in the glass surface-to-volume ratio did not cause an observable change in reaction rates.

(124) Pimblett, G.; Garner, C. D.; Clegg, W. *J. Chem. Soc., Dalton Trans.* **1985**, 1977.

of $[(Ph_3P)_3Rh(MeCN)]^+$ (see above). (c) A solution of **1** (20 mg) and PPh_3 (100 mg) in a mixture of benzene (0.7 mL) and $PhNO_2$ (0.2 mL) was kept at 45 °C for 1 h, and then analyzed by ^{19}F NMR. The analysis indicated ca. 15% conversion to **5**. No formation of **3** was noticed. Under similar conditions but in the absence of $PhNO_2$, ca. 30% conversion to **5** was observed. (d) A solution of **5** (22 mg) and PPh_3 (95 mg) in a mixture of benzene (0.7 mL) and $PhNO_2$ (0.2 mL) was kept 25 °C for 1 h, and then analyzed by ^{19}F NMR. The analysis indicated ca. 80% conversion to **1**. No formation of **3** was noticed, although a small amount (ca. 5%) of a P–F species (-74.7 ppm, dd, $J_{F-P} = 1017$ Hz, $J_{F-Rh(P)} = 9$ Hz) was observed. Under similar conditions but in the absence of $PhNO_2$, no conversion to **1** (<5%) was observed.

X-ray Crystallographic Studies. A summary of crystallographic data for new complexes **3**, **5**· $2C_6H_6$, **5**· Et_2O , and **6** is presented in Table 5. The CIF files are presented in the Supporting Information.

Computational Studies. Details of computational studies are presented in the Supporting Information.

Acknowledgment. This is DuPont CR&D contribution no. 8591. S.A.M. thanks Heriot-Watt University and the EPSRC for funding. Computational resources on a HP/COMPAQ ES40 multiprocessor cluster (Columbus) at the Rutherford Appleton Laboratory (RAL), provided by the EPSRC National Service for Computational Chemistry Software, are acknowledged.

Supporting Information Available: Details of kinetic, crystallographic (CIF), and computational studies. This material is available free of charge via the Internet at <http://pubs.acs.org>.

JA054506Z